coatings

MDPI

Article

Curcuma longa Mediated Synthesis of Copper Oxide, Nickel Oxide and Cu-Ni Bimetallic Hybrid Nanoparticles: Characterization and Evaluation for Antimicrobial, Anti-Parasitic and Cytotoxic Potentials

Shah Faisal [1,*], Najlaa S. Al-Radadi [2], Hasnain Jan [1,3,*], Abdullah [4], Sajjad Ali Shah [1], Sumaira Shah [5], Muhammad Rizwan [6], Zobia Afsheen [7], Zahid Hussain [6], Muhammad Nazir Uddin [6], Muhammad Idrees [8] and Nadia Bibi [9]

1 Institute of Biotechnology and Microbiology, Bacha Khan University, Charsadda 24460, Pakistan; sajjadbiotec@gmail.com
2 Department of Chemistry, Taibah University, Al-Madinah Al-Munawarah 14177, Saudi Arabia; nsa@taibahu.edu.sa
3 Department of Biotechnology, Quaid-i-Azam University, Islamabad 45320, Pakistan
4 Department of Microbiology, Abdul Wali Khan University, Mardan 23200, Pakistan; abdull9393@gmail.com
5 Department of Botany, Bacha Khan University, Charsadda 24460, Pakistan; sunehra2233@gmail.com
6 Centre for Biotechnology and Microbiology, University of Swat, Khyber Pakhtunkhwa 19120, Pakistan; muhammad.rizwanbiotec@gmail.com (M.R.); zahid11@gmail.com (Z.H.); nazir55@gmail.com (M.N.U.)
7 Department of Biotechnology and Microbiology, Abasyn University Peshawar, Khyber Pakhtunkhwa 25000, Pakistan; zobia96@gmail.com
8 Department of Biotechnology, University of Swabi, Khyber Pakhtunkhwa 94640, Pakistan; idrees42@gmail.com
9 Department of Microbiology, Shaheed Benzair Bhutto Women University, Peshawar 00384, Pakistan; nadia39@yahoo.com
* Correspondence: shahfaisal11495@gmail.com (S.F.); rhasnain849@gmail.com (H.J.); Tel.: +92-315-9353-867 (S.F.); +92-305-8464-348 (H.J.)

check for updates

Citation: Faisal, S.; Al-Radadi, N.S.; Jan, H.; Abdullah; Shah, S.A.; Shah, S.; Rizwan, M.; Afsheen, Z.; Hussain, Z.; Uddin, M.N.; et al. *Curcuma longa* Mediated Synthesis of Copper Oxide, Nickel Oxide and Cu-Ni Bimetallic Hybrid Nanoparticles: Characterization and Evaluation for Antimicrobial, Anti-Parasitic and Cytotoxic Potentials. *Coatings* **2021**, *11*, 849. https://doi.org/10.3390/coatings11070849

Academic Editor: Aldona Balčiūnaitė

Received: 18 May 2021
Accepted: 6 July 2021
Published: 14 July 2021
Corrected: 28 December 2023

Publisher's Note: MDPI stays neutral with regard to jurisdictional claims in published maps and institutional affiliations.

Abstract: Nanoparticles have long been known and their biomedical potent activities have proven that these can provide an alternative to other drugs. In the current study, copper oxide, nickel oxide and copper/nickel hybrid NPs were biosynthesized by using *Curcuma longa* root extracts as a reducing and capping agent, followed by characterization via UV-spectroscopy, Fourier transformed infrared spectroscopy (FTIR), energy dispersive X-ray (EDX), powder X-ray diffraction (XRD), scanning electron microscopy (SEM), transmission electron microscopy (TEM), thermo galvanometric analysis (TGA), and band gap. FTIR spectroscopy shows the availability of various functional groups and biomolecules such as carbohydrate, protein, polysaccharides, etc. The EDX peak confirmed that the elemental nickel and copper were present in large quantity in the analyzed sample. Scanning electron micrographs showed that the synthesized CuO-NPs and NiO-NPs were polyhedral uniform and homogeneous in morphology, while the copper/nickel hybrid NPs were well dispersed, spherical in shape, and uniform in size. TEM micrographs of CuO-NPs had 27.72 nm, NiO had 23.13 nm and, for their hybrid, the size was 17.38 nm, which was confirmed respectively. The CuO and NiO NPs possessed spherical- to multi-headed shapes, while their hybrid showed a complete spherical shape, small size, and polydispersed NPs. The XRD spectra revealed that the average particle size for CuO, NiO, and hybrid were 29.7 nm, 28 nm and 27 nm, respectively. Maximum anti-diabetic inhibition of (52.35 ± 0.76: CuO-NPs, 68.1 ± 0.93: NiO-NPs and 74.23 ± 0.42: Cu + Ni hybrids) for α-amylase and (39.25 ± 0.18 CuO-NPs, 52.35 ± 1.32: NiO-NPs and 62.32 ± 0.48: Cu + Ni hybrids) for α-glucosidase were calculated, respectively, at 400 µg/mL. The maximum antioxidants capacity was observed as 65.1 ± 0.83 µgAAE/mg for Cu-Ni hybrids, 58.39 ± 0.62 µgAAE/mg for NiO-NPs, and 52.2 ± 0.31 µgAAE/mg for CuO-NPs, respectively, at 400 µg/mL. The highest antibacterial activity of biosynthesized NPs was observed against *P. aeuroginosa* (28 ± 1.22) and *P. vulgaris* (25 ± 1.73) for Cu + Ni hybrids, respectively. Furthermore, the antibiotics were coated with NPs, and activity was noted. Significant anti-leishmanial activity of 60.5 ± 0.53 and 68.4 ± 0.59 for Cu + Ni hybrids;

53.2 ± 0.48 and 61.2 ± 0.44 for NiO-NPs; 49.1 ± 0.39 and 56.2 ± 0.45 for CuO-NPs at 400 µg/mL were recorded for promastigote and amastigotes, respectively. The biosynthesized NPs also showed significant anti-cancerous potential against HepG2 cell lines. It was concluded from the study that NPs are potential agents to be used as an alternative to antimicrobial agents.

Keywords: *Curcuma longa*; copper oxide nanoparticles; nickel oxide nanoparticles; urinary tract infections; green synthesis

1. Introduction

Nanotechnology is now recognized as an established cutting-edge technology with a wide range of applications in the pharmaceutical and other industries [1]. Many nanoscale devices have been developed using a number of methods since the dawn of nanotechnology. In recent ages, the environmentally friendly 'green' production of nanomaterials is becoming an essential and popular focus for material scientists as a result of widespread noxious problems associated with chemical and physical techniques. The plant-mediated synthetic approach, on the other hand, is a valuable technique that can be conveniently manufactured and engineered [2–5]. Standard approaches to nanoparticle synthesis have a number of disadvantages, including long-term production, high costs, time consuming methods, and the use of toxic compounds, in particular. Because of these limitations, the majority of related research has concentrated on environmentally sustainable and fast synthesis protocols for nanoparticle processing [6–9]. In recent years, material science has prioritized the advancement of environmentally friendly methods for synthesizing nanoscale materials. A green synthetic approach for NPs, especially using various plant extracts, is a growing trend in green chemistry that is easy, inexpensive, and non-toxic in this regard [10–12]. Nanoscale technology has since improved the human quality of living by addressing a variety of issues such as industrial prosperity, climate change, food, clothes, and healthcare, as well as the treatment of lethal diseases such as cancer, respiratory infections, and Alzheimer's disease [13,14].

Over the past ten years, metal oxide NPs have been used most widely for their myriad of applications in various chemical, physical, and biological fields. Metal oxide nanoparticles have been the subject of extensive research over the past decade due to their diverse uses in a variety of scientific fields [15]. Materials like (Cu and Ni) NPs are exciting, inorganic materials with many advantages. Energy management, textiles, batteries, health care, catalysis, cosmetics, semiconductors, and chemical sensing are only a few of the applications for (Cu and Ni) NPs [16–18]. These metallic NPs are non-toxic, biocompatible, and have a wide range of medicinal uses, including anti-cancer [19], anti-inflammation [20], antimicrobial selective drug delivery [21], wound healing, and bio-imaging [22,23].

Nanoproducts can be manufactured using a number of approaches (chemical, physical, and biosynthesis), and have a wide range of properties and applications. Although the synthesis of plant-based NPs (CuO, NiO and Cu/Ni hybrid) has been documented above, there is a lack of antimicrobial, antioxidant, anti-leishmanial, and anti-cancer effects among other biological properties in the literature. *Curcuma longa* is well known for its medicinal properties, which include anti-inflammatory, anti-diarrheal, dyspepsia, depression, and mood disorders [24–27].

Using the aqueous extracts of *Curcuma longa* root extract, we recorded the plant-based synthesis of copper oxide, nickel oxide, and copper/nickel hybrid nanoparticles. The environmentally sustainable synthesis of such metallic NPs has a variety of biomedical applications. The metabolites in *C. longa's* aqueous extract served as oxidizing and reducing agents, as well as a strong capping agent, in the synthesis of biogenic NPs. Modern techniques such as FTIR, UV, XRD, SEM, TEM, and TGA analysis were used to characterize the green synthesized nanoparticles. The NPs were then tested for antimicrobial, anti-leishmanial, anti-diabetic, antioxidant, and anti-cancer properties.

2. Materials and Methods

2.1. Plant Collection and Extraction

The roots of *C. longa* were found and purchased in a local market of Charsadda, Pakistan, and stored with CL001 tag number at Department of Botany Herbarium, Bacha Khan University, Pakistan. For extract preparation, the specimen was washed thrice with sterile water and ground into a fine powder using an electric grinder. Next, 50 g of fine root powder were mixed to 500 mL dH_2O before being heated at 100 °C for half an hour, followed by incubation at room temperature overnight. The concentrate was filtered using Whatman filter paper. The collected extract was held at 4 °C in the refrigerator for further use in the experiment.

2.2. Synthesis of CuO and NiO NPs

Copper oxide nanoparticles were synthesized using a modified version of a previously mentioned technique [28]. Exactly 6.0 g of cupric acetate $Cu(CH_3COO)_2$ (Sigma–Aldrich, Saint Louis, MO, USA) was applied to 100 mL extract and held at 60 °C for 2 h on a magnetic stirrer. After the reaction was finished, the mixture was cooled at 25 °C before being centrifuged (HERMLE Z326K, HERMLE Labortechnik GmbH, Wehingen, Germany) at 10,000 rpm for 10 min. The resulting pellet was washed three times with purified water before being poured onto a clean Petri plate and dried in the oven at 90 °C. To remove any impurities, the dry material was pounded into a fine powder in a pestle and mortar and calcined for 2 h at 500 °C. The resulting product was stored for physiochemical characterization. With minor modifications, nickel oxide nanoparticles were synthesized according to a previously mentioned procedure [29]. Then, 6.0 g of Nickel(II) acetate (Sigma –Aldrich, Saint Louis, MO, USA) was mixed to 100 mL extract of plant and held at 60 °C for 2 h on a magnetic stirrer and same procedure was repeated as above discussed in the synthesis of CuO nanoparticles. The resulting NiO nanoparticles were stored at 4 °C in a refrigerator for physiochemical characterization.

2.3. Synthesis of Cu-Ni Hybrids NPs

Hybrid nanoparticles were made using a modified version of a previously mentioned protocol [30]. Precisely 50 mL of distilled water was combined with 3.0 g of both salt cupric acetate and Nickel (II) acetate. Both 50 mL aqueous solution of metallic salts were mixed together and held at 60 °C for 2 h on a magnetic stirrer. Following that, 100 mL of extract was applied to the salts solution dropwise. After the reaction was finished, the mixture was able to cool at 25 °C before being centrifuged at 10,000 rpm for 10 min. The resulting pellet was washed three times with purified water before being poured onto a clean Petri plate and dried in the oven at 90 °C. To remove any impurities, the dry material was pounded into a fine powder in a pestle and mortar and calcinated for 2 h at 500 °C. The resulted product was stored for physiochemical characterization.

2.4. Characterizations of Biosynthesized NPs

Advanced characterization techniques have been used for determining the physico-chemical characteristics of *C. longa* mediated NPs. UV, FTIR, XRD, SEM, TEM, EDX, and TGA are the techniques used for the physiochemical characterization of the biosynthesized NPs. UV spectroscopy (Spectrophotometer UV5, Mettler-Toledo, Colombus, OH, USA) in the range of 200 to 700 nm was used to examine the reaction between the extract and metallic salts. The crystalline nature of the biosynthesized NPs were confirmed by PANalyticaX'pert X-ray diffractometer (Malvern Panalytical, San Francisco, CA, USA) in XRD analysis. The crystal size was calculated by Scherer's equation [31].

$$D = k\,\lambda/\beta\,\mathrm{Cos}\theta$$

A 400 cm^{-1} and 4000 cm^{-1} spectral range was used to examine the possible involvement of functional groups in the formulation of NPs in FTIR (Shimadzu, Tokyo, Japan)

analysis. SEM (JSM-7600F, JOEL, Ltd., Tokyo, Japan) and TEM (JEM-2100F, JEOL Ltd., Tokyo, Japan) were used to analyze morphology and physical measurements, while elemental analysis was performed using EDX Spectroscopy (Shimadzu, Tokyo, Japan) [32]. Thermo gravimetric analysis was used to investigate thermal equilibrium/stability using a Q500 thermo gravimetric analyzer (TGA Thermostep, Eltra Elemental Analyzers, Haan, Germany).

2.5. Antibacterial Assay of NPs against Bacterial Strains

Previously identified bacterial species (*Escherichia coli, Pseudomonas aeruginosa, and Proteus vulgaris*) were collected from the Hayat Abad medical Complex (HMC), Peshawar. The collected bacterial species were used to determine the antibacterial potential of biosynthesized NPs. Different antibiotic discs were used in the current study according to CLSI guidelines (CLSI, 2017 and 2020), including imipenem, meropenem, oxacillin, and ciprofloxacin against test organisms. Agar well diffusion assay [33] was performed to evaluate the antimicrobial potential of Cu, Ni, and Cu-Ni hybrid nanoparticles against *Proteus vulgaris*, *Pseudomonas aeruginosa*, and *Escherichia coli*. Next, 0.5 OD MacFarland microbial suspension were prepared. Then, 50 µL of microbial culture was pipetted out and dropped on freshly prepared Muller–Hinton agar plates to form a uniform bacterial lawn by spread plate technique. After that, a sterilized well-borer was used for boring a well of 6–5 mm, and 10 µL of nanoparticles were pipetted out and poured into each well in each plate and labeled accordingly. Ciprofloxacin was used as a positive control 177 while deionized water was used as a negative control. The plates were incubated for 24 h at 37 °C and, after incubation, inhibition zones were measured by using a vernier caliper. The same process was repeated for each nanoparticle.

2.6. Anti-Leishmanial Assay

Using the standard protocol mentioned previously, biogenic NPs were tested for anti-leishmanial action against both amastigotes and promastigotes [34]. The anti-leishmanial behavior of biogenic nanoparticles was evaluated using the *L. tropica* KWH23 strain. The cultured *L. tropica* KWH23 strain in the FBS-supplemented MI99 medium, was incubated. Next, 20 µL of the test sample was poured into a 96-well plate, followed by an additional 180 µL of aliquot from suspension culture (seeding density: 1×10^6 cells/mL), and was incubated for 3 days at 25 °C. Amphotericin B and DMSO (1%) was used as positive and negative control. After that, 20 µL of MTT solution (4 mg/mL in dH_2O) were poured into each well and the culture plate was incubated for another four hours at room temperature. The absorbance of the samples was measured at 540 nm using a microplate reader. Percent inhibition was calculated using the formula

$$\% \text{ Inhibition} = \left[1 - \left\{\frac{\text{Absorbance of sample}}{\text{Absorbance of control}}\right\}\right] \times 100$$

The sample was analyzed again using different a concentration and the process was repeated three times. The IC_{50} values were revealed by using TableCurve software 2D v5. 01.

2.7. Protein Kinase Inhibition Assay

Protein kinase inhibition assay was used to test the anti-cancer potential of CuO, NiO, and its hybrid NPs. This is a bioassay for confirming the ability of nanoparticles to suppress protein kinases. Our procedure differed marginally from that adopted by [35]. Streptomyces 85E was used as a research strain. We made the plates with sterile ISP4 medium and then moved a volume of 100 µL from the Streptomyces 85E culture that had been refreshed to the plates. Each well (5 mm) was filled with around 5 µL of NPs and labelled accordingly. Surfactin was used as a positive control, while DMSO was used as a negative control. Followed by incubation after this, all the plates were set at 28 °C for 48 h. Clear and bald areas were observed around wells, which indicated that phosphorylation, mycelia, and spore formation had been inhibited. The clear zones displayed the cytotoxic

potential of NPs and the killing of the test strain, and the clear zones were measured with a vernier caliper to the nearest mm.

2.8. Cytotoxicity against HepG2 Cell Line

HepG2 cells (ATCC HB-8065) were cultured at 37 °C in Dulbecco's Modified Eagle Medium (DMEM) containing 10% Fetal Calf Serum (FCS), 100 U/mL penicillin, 2 mM L-glutamine, 100 µg/mL streptomycin, and 1 mM Na-pyruvate in a 5% humified CO_2 atmosphere. The cells were harvested for 1 min at room temperature with 0.5 mM trypsin/EDTA. The cytotoxic activity of nanoparticles in vitro was investigated using MTT (3-4,5-dimethylthiazol-2-yl)-2,5-diphenyltetrazolium bromide, a tetrazolium dye. MTT is reduced in healthy cells to formazan, an insoluble purple substance that can be measured spectrophotometrically. Exactly 200 µg/mL of the test sample was added to 10,000 cells/well of HepG2, followed by an additional 10 µL MTT dye and then incubated for 3 h. After that, the cells were incubated for an overnight period. Using a microplate reader, plates were analyzed at 570 nm (Platos R 496, AMP, Krenngasse, Austria). As a control, non-treated HepG2 cells were used. As a negative control, DMSO was used. The following formula was used to quantify percent viability in comparison to the NTC study:

$$\% \text{ Viability} = \frac{\text{Absorbance of sample} - \text{Absorbance of sample control}}{\text{Absorbance of NTC} - \text{Absorbance of media}} \times 100.$$

Optical density of treated samples and NTC was measured at 570 nm. Abs of sample control and Abs of blank represent the background optical density; the former was measured in test sample/extracts only while the latter was measured in media only samples.

2.9. Anti-Diabetic Assay

The anti-diabetic efficacy of the biogenic NPs was calculated using alpha amylase and glucosidase inhibition assays.

2.9.1. α-amylase Inhibition Assay

We used the most appropriate protocol with few small modifications for the assessment of alpha amylase inhibition potential on biogenic NPs [36]. This assay was carried out in a 96-well microplate. Next, 15 µL of PBS, 25 µL of enzyme, NPs (10 µL), and 40 µL of starch were poured into each well and incubated at 50 °C. Followed by incubation, 20 µL of HCL and 90 µL I_2 were added to each well. We used DMSO as a negative control and acarbose as a positive control. The sample absorbance potential was measured using a microplate photometer set to 540 nm. Using the following algorithm, we determined the percentage inhibition:

$$\% \text{ Enzyme inhibition} = \left(\frac{\text{Abs Sample} - \text{Abs negative control}}{\text{Abs blank} - \text{Abs negative control}} \right) \times 100$$

2.9.2. α-glucosidase Inhibition Assay

The anti-diabetic efficacy of NPs was further assessed using a previously published -glucosidase inhibition bioassay with minor changes [37,38]. Exactly 50 mL of alpha glucosidase PBS were combined with 100 mg of bovine serum albumin. A reaction mixture constituting 10 µL of tested sample, phosphate buffer (490 µL; pH 6.8), and *p*-nitrophenyl α-D-glucopyranoside (5 mM; 250 µL) was kept for incubation at 37 °C for 5 min. Next, 250 µL α-glucosidase (0.15 unit/mL) was then introduced to samples, followed by incubation for 15 min at 37 °C. Absorptions were measured using a UV-Vis spectrophotometer at 400 nm after the reaction was stopped by applying a 2 mL Na_2CO_3 (200 mM) solution. The p-nitrophenol-released *p*-nitrophenyl and α-D-glucopyranoside were measured in this

assay. Acarbose was used as a constructive control in the experiment, which was repeated three times.

$$\% \text{ Enzyme inhibition} = \left(\frac{Abs\ Sample - Abs\ negative\ control}{Abs\ blank - Abs\ negative\ control} \right) \times 100$$

2.10. Anti-Alzheimer's Activity

Inhibition of the enzymes Acetylcholinesterase (AChE) and Butyrylcholinesterase (BChE) may be a target in Alzheimer's treatment. The ability of NPs to inhibit AChE (Sigma "101292679") and BChE (Sigma "101303874") was investigated using Elman's technique with minor modifications, as previously mentioned [39]. The test sample was applied in a concentration range of 12.5 µg/mL to 400 µg/mL. Briefly, NPs were dispersed in phosphate buffer saline (PBS) solution. The final concentration of the enzyme in AChE was 0.03 U/mL and 0.01 U/mL in BChE. The reaction mixture prepared in distilled water included DTNB (0.00022M), BTchI (0.0005M), and ATchI (0.0005M), and was stored at 8 °C. Methanol mediated Galanthamine hydrobromide (Sigma; GI660) was taken as positive control while the reaction mixture deprived of test sample was used as negative control. The anticholinesterase assay works by hydrolyzing ATchI into AChE and BTchI into BChE, which results in the formation of the 5-thio-2-nitrobenzoate anion and forms further complexes with DTNB, resulting in a yellow color. Absorbance was measured using a UV spectrophotometer set to 412 nm. With a difference in absorption rate over time, Galantamine and NPs can be used to calculate percent enzyme inhibition and percent enzyme activity.

2.11. Estimation of Antioxidant Activity

2.11.1. DPPH Antioxidant Assay

The antioxidant function of DPPH (2,2-diphenyl-1-picrylhydrazyl) and FRSA (free radical scavenging assay) was calculated using the protocol [40], with minor modifications. Sample extract (20 µL) was combined with DPPH (3.2 mg/100 mL methanol) 180 µL, and the mixture was incubated at 25 °C for 60 min before adding dH_2O (160 µL). The absorbance at 517 nm was measured using an absorbance microplate reader (BioTek ELX800 Absorbance Microplate Reader, BioTek Instruments, Colmar, France). The methanolic extract and 0.5 mL of DPPH solution were used as standards to map the calibration curve (R^2 = 0.989). The free radical scavenging operation was measured using the following equation as a percentage of DPPH discoloration:

$$Free\ radical\ scavenging\ activity(\%) = 100 \times \left(1 - \frac{Ac}{As}\right)$$

2.11.2. Total Antioxidant Capacity Determination (TAC)

The same assay as stated by [41] was used to examine overall antioxidant ability by using a micropipette to pour 100 microliters of NPs into Eppendorf tubing. Then, we fill Eppendorf tubes with 900 µL TAC, followed by incubation for only two hours at 90 °C; the absorbance of the sample was observed at 630 nm.

2.11.3. Total Reducing Power Determination (TRP)

The same method as described by [42] was used to determine the total reducing power (TRP). The 100 microliter of test sample was poured into Eppendorf tube, followed by the addition of PBS and potassium ferric cyanide and incubated for half an hour at 50 °C. The centrifugation was performed and collected supernatant were shifted into a 96-well plate and observed at an absorbance of 630 nm.

2.11.4. Antioxidant ABTS Assay

The previous technique was used for the evaluation of this assay [41]. Briefly, the ABTS was made by combining 7 mM ABTS salt with 2.45 mM potassium persulphate in

an equal proportion and storing the mixture in the dark for 16 h. Before combining with extracts, the solvent absorbance was measured at 734 nm and calibrated to 0.7. The mixture was then placed in the dark for another 15 min at room temperature (25 °C).

2.12. Biocompatibility Studies

Fresh erythrocytes were used to show the biocompatibility of biogenic metallic NPs [43]. After the individual's consent, 1 mL of blood was taken in EDTA tubes from healthy individuals. To isolate RBCs, the sample was centrifuged and the pellets were retrieved after three washes with PBS. PBS-erythrocyte suspension was then made, combined with NPs, and incubated. The sample was centrifuged after incubation and 200 microliters of supernatant was shifted into 96-well plate, and the release of hemoglobin was observed at 450 nm. The formula for calculating percent hemolysis was:

$$\text{〃(\%) Haemolysis } = \left(\frac{sample\ Ab - negative\ control\ Ab}{Positive\ control\ Ab - Negative\ control\ Ab} \right) \times 100$$

3. Results and Discussion

3.1. Biosynthesis of Metallic NPs

Curcuma longa is known as "turmeric" and belongs to family *Zingiberaceae* [44]. From previous literature, numerous therapeutic activities have been assigned to *C. longa* for a wide variety of diseases and conditions including those of the skin, pulmonary and gastrointestinal systems, aches, pains, wounds, sprains, and liver disorders. Extensive research within the last half-century has proven that most of these activities, once associated with *C. longa*, are instead due to curcumin. Curcumin, with a percentage of 10.3% in the extract, has been shown to exhibit antioxidant, anti-viral, anti-inflammatory, antibacterial, antifungal, and anti-cancer activities, and thus has a potential against various malignant diseases, diabetes, allergies and Alzheimer's. Curcumin is the most important fraction which is responsible for its biological activity. The phenolic content of *C. longa* extract was found to be 11.24 mg GAE/g. Pharmaceutically important phytochemicals including alkaloids, flavonoids, terpenoids, steroids, saponins, phenols, glucosides, etc., were found to be present in extracts of *C. longa* [45]. Metallic nanoparticles were synthesized using *C. longa* extract as a capping and reducing agent. When the reaction was carried out between *C. longa* and respective salts, the color of the mixture changed from dark brown to black and dark gray, which confirmed the biosynthesis of CuO-NPs, NiO-NPs, and Cu-Ni alloy NPs [46–48]. The reaction mixture was centrifuged and stored for physiochemical characterization [49].

3.2. Optical Band Gap of Nanoparticles

The optical band gap of CuO, NiO, and its hybrid nanoparticles, was determined using the basic relationship between absorbance and incident photon energy ($h\nu$), as shown in the Figure 1. The band gap of CuO-NPs was calculated as 3.0 eV, while that of NiO-NPs was determined as 2.6 eV; for hybrid, the band gap calculated was 2.48 eV, respectively. (Beckman model DB). The smaller band gap results in enhanced photo degradation activity, in which the electrons are easily excited from the valence to conduction band [19].

3.3. Fourier Transform Infrared Spectrometer (FTIR)

To find out the possible reducing agent responsible for generation of NPs, FTIR analysis was carried out. In current findings, the FTIR spectra of CuO, NiO and its hybrid are shown in Figure 2 (IRAffinity-1S). The different absorption bands were observed at 1599, 1408, 1081, 565 for CuO-NPs [50]. The absorption band at 1599 cm^{-1} is due to the in-plane CH bending vibration from the phenyl rings while 1408, 1081 and 565 cm^{-1} represent the presence of CH3, ref. [51] stretch phosphate originate from phosphodieaster bond of nucleic acids and Phenyl ring respectively. The NiO-NPs shows different absorption bands at different wavelength. The absorption band at 1603 and 1587 revealed the symmetric CH_3

bending modes of the methyl groups of proteins. The absorption bands at 1418, 1076 and 596 shows the presence of polysaccharides (pectin) with COO_2, C=C and C-OH_3 torsion of methoxy group respectively. The hybrid NPs of both metals shows the presence of different functional groups at 1604, 1387, 1221, 1028 and 768. These absorption bands show the presence of CH_3, Phosphate II, glycogen and guanine [52]. These functional groups are due to C-O and C-C stretching and C-O-H deformation motions. From the above spectroscopic analysis of CuO-NPs and NiO-NPs and its hybrid it is concluded that various functional groups are present in plant extract of *Curcuma longa.* These functional groups holding a promising role in reduction as well as stabilizing the reaction medium.

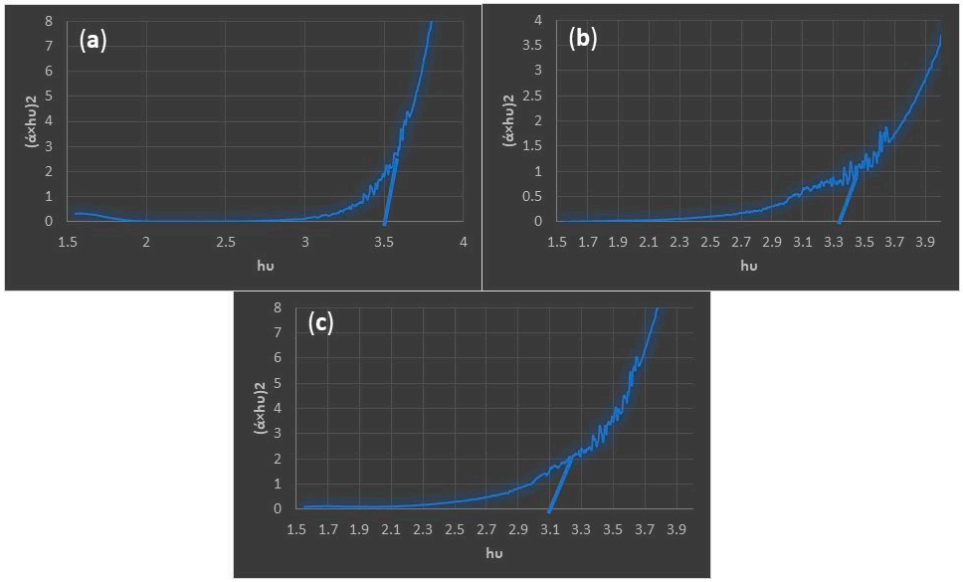

Figure 1. Band gap of *Curcuma longa* synthesized NPs (**a**) CuO, (**b**) NiO and (**c**) Cu/Ni hybrids.

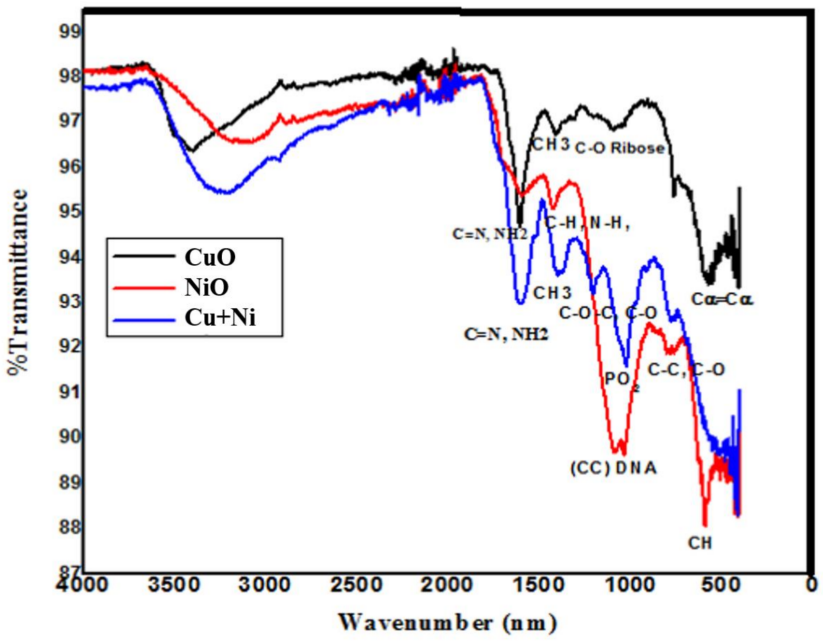

Figure 2. Typical FTIR spectra of CuO, NiO, and Cu/Ni hybrds.

3.4. Powder XRD Analysis

As shown in Figure 3, the XRD spectra shows an intense peak at 43.30 which, having plane (111), is crystalline plane for Cu and matched with bulk Cu (Model-D8 Advance, Germany) [53]. Other low intensity peaks at 2θ values 36.6, 55.5, and 64.5 matched with planes (002), (110) and (220), respectively. All of these planes are close to JCPDS File No. 5-0661. The matching plane indicated that the prepared CuO-NPs are highly crystalline in nature. The size was calculated as 29.7 nm by using the Debye–Scherrer equation. The same planes of index were also found for NiO-NPs and no such peak was observed due to impurities. The average particle size of NiO-NPs was 28 nm, calculated by using the Debye–Scherrer formula. The peak positions at 2θ values for hybrid of both CuO and NiO NPs were at 31.6, 45.5, and 62, with matching planes (100), (200) and (220), respectively. The average calculated hybrid nanoparticle size was 27 nm. The comparative size and nature study revealed that, compared to NiO/CuO nanoparticles, the hybrid of both showed a small particle size and were monoclinic in nature.

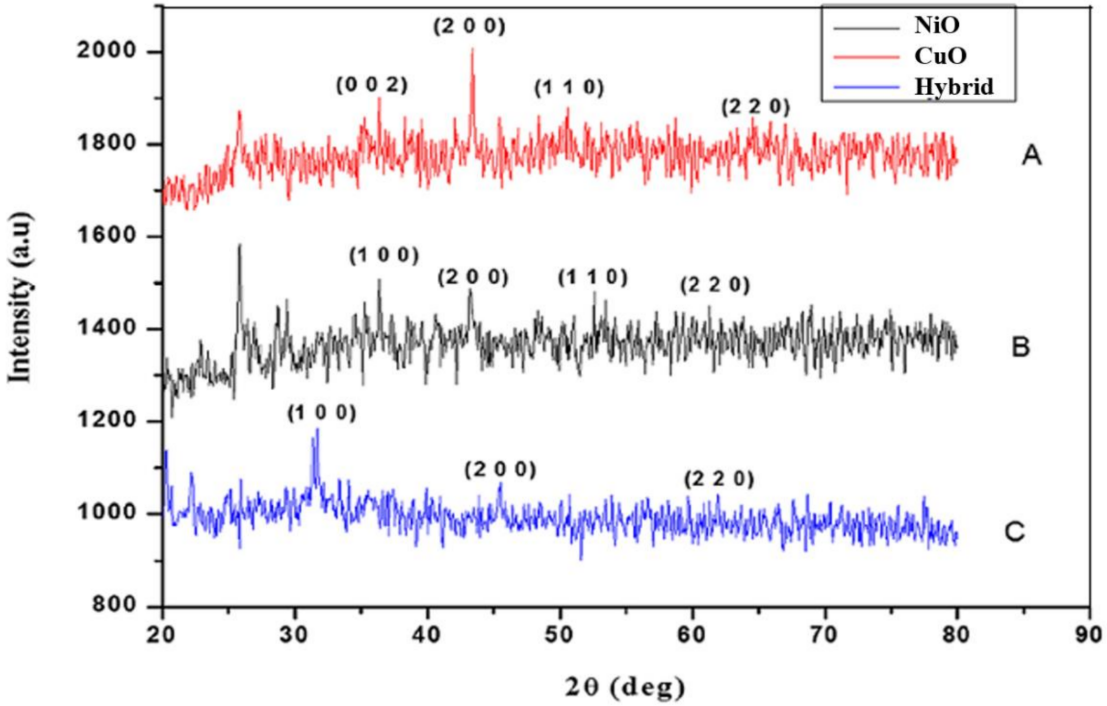

Figure 3. XRD graph of *Curcuma longa* synthesized: (**A**) CuO, (**B**) NiO and (**C**) Cu + Ni hybrids.

3.5. Thermal Properties

Thermal properties of the biosynthesized nanoparticles were studied using thermal gravimetric (TGA) analysis in a temperature range from 25 °C up to 600 °C, as shown in Figure 4 (TGA-55-TA). The total weight loss of the CuO-NPs was recorded as 63% until 600 °C, while NiO-NPs resulted in only 69% weight loss, and the hybrid NPs total loss was observed as 59.3%. The initial weight loss up to 150 °C is attributed to the dehydration and loss of moisture content from the samples [54]. Our results thus indicated that biosynthesized hybrid are thermally more stable than NiO-NPs, and NiO-NPs are more stable than CuO-NPs.

3.6. Energy Dispersive X-rays (EDX)

The current findings were also tested for the presence of elements in synthesized Cu/Ni and its hybrid-NPs (JSM 7400F, JEOL Ltd., Tokyo, Japan). The EDX analysis showed the presence of Cu and Ni in large quantity. The EDX spectroscopy of hybrid (Cu/Ni its hybrid-NPs) showed the presence of both Cu and Ni. Some other trace elements like iron

(Fe) and sulfur (S) were also present due to handling during experiment. The presence of other elements like oxygen, potassium, sodium, and nitrogen were due to plant extract biomolecules, as shown in Figure 5.

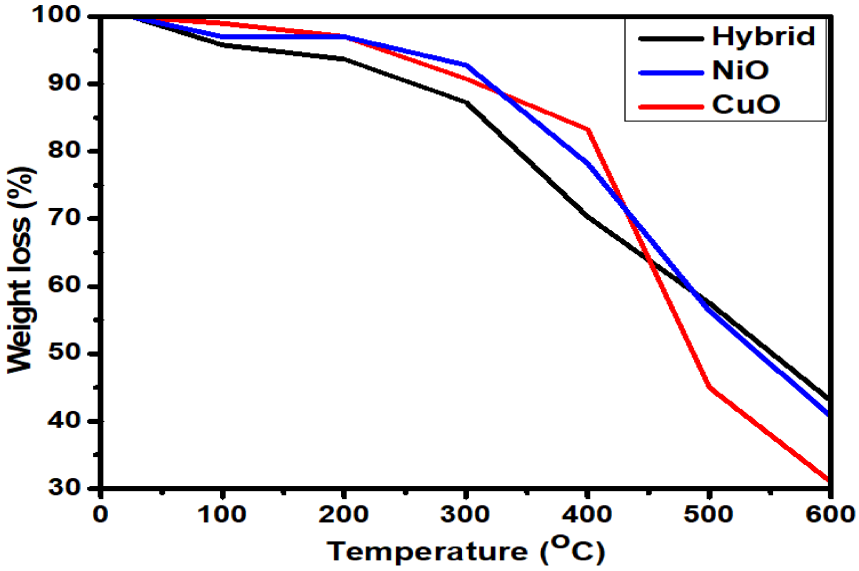

Figure 4. TGA analysis of CuO-NPs, NiO-NPs and Cu/Ni hybrids.

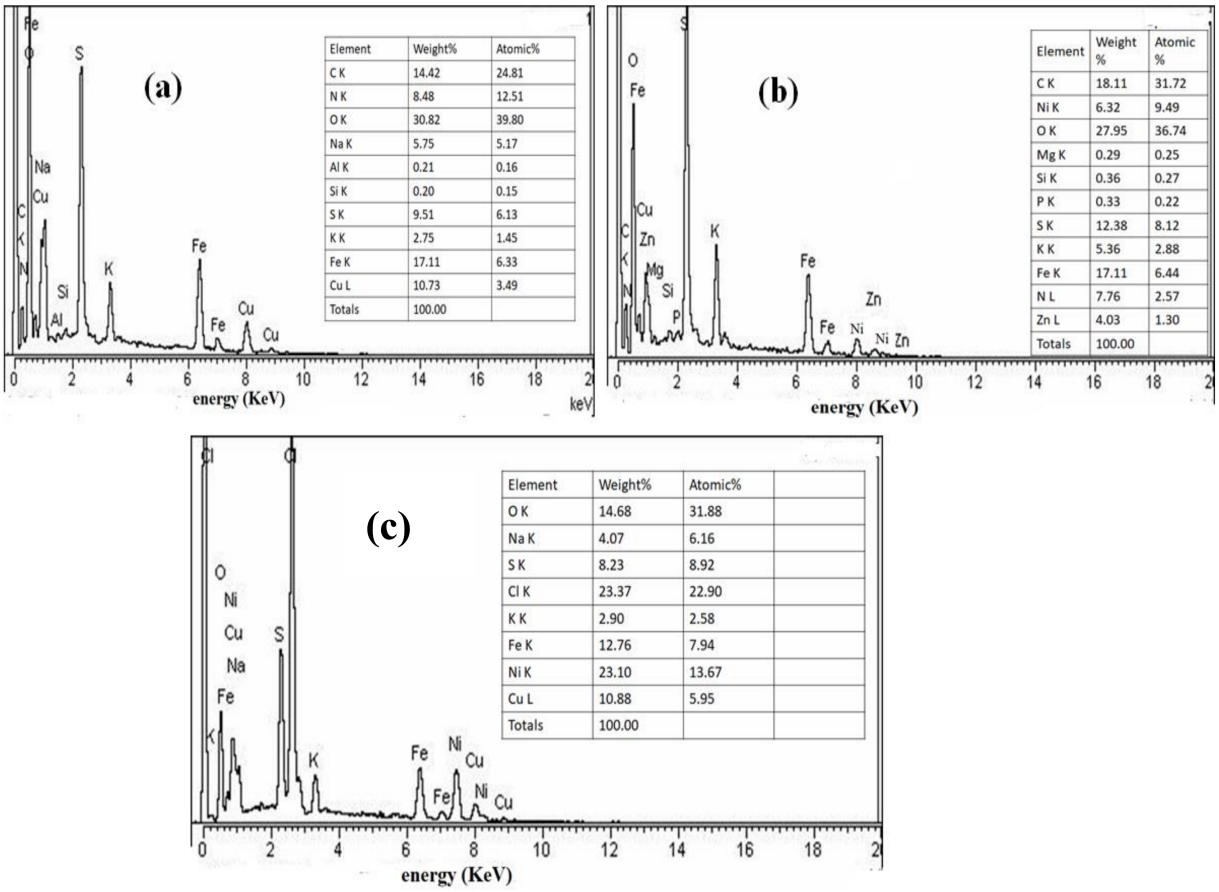

Figure 5. EDX spectra of *Curcuma longa* mediated NPs (**a**) CuO-NPs, (**b**) NiO-NPs and (**c**) Cu + Ni hybrids.

3.7. Morphological SEM and TEM Analysis

The morphological study of CuO, NiO, and its hybrid was carried out by scanning electron microscopy. Micrographs showed that the NPs of CuO and NiO are non-spherical polyhedral-shaped and polydispersed in reaction medium [55,56]. The morphological feature of hybrid shows a smooth surface, spherical shape, and small sized particles as shown in Figure 6 [49]. SEM micrographs of the CuO, NiO, and its hybrid NPs revealed agglomerated morphology, with the larger mean size of the powdered samples (JSM-7600F, Japan). The TEM image and electron diffraction pattern of the CuO, NiO, and its hybrid NPs are presented in Figure 7 (JEM-2100F, JEOL Ltd., Tokyo, Japan). TEM micrographs showed a spherical or elliptical morphology of the synthesized NPs, with a mean size of 27.72 for CuO-NPs, while for NiO-NPs the size was 23.13, and for their hybrid, the calculated size was 17.38, respectively [10,57]. The dimensions of about 50 particles were calculated for each sample using ImageJ software. The particles size of CuO, NiO and its hybrid NPs were in agreement with that of XRD analysis.

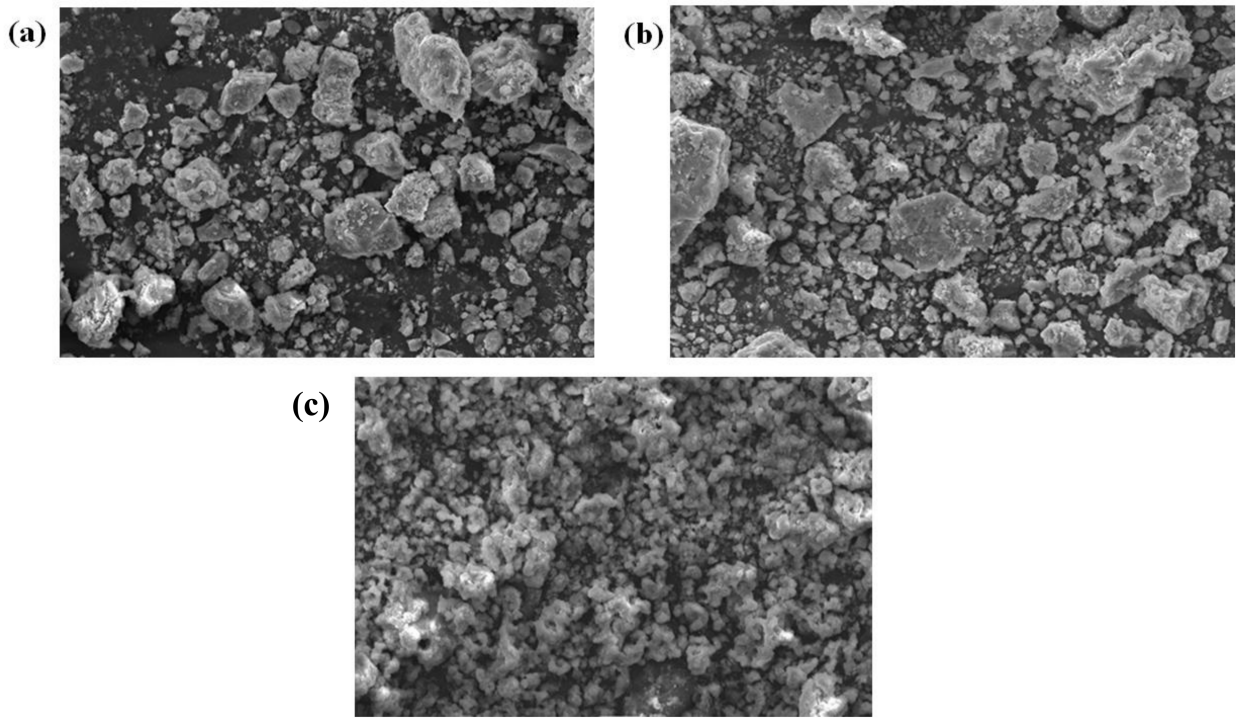

Figure 6. SEM micrograph of *Curcuma longa*: (**a**) CuO, (**b**) NiO and (**c**) Cu/Ni hybrids.

3.8. Antibacterial Assay

Antibiotic resistance is a major problem that continues to affect a large portion of the world [58]. Plant-mediated nanomaterials have proven significant as a result of their antimicrobial properties [59–61]. Phytochemicals have developed into a unique synthesis technique for nanoparticles, as they serve both as reducing and capping agents for the nanoparticles [62]. In this research, we used *Curcuma longa* extract to produce various nanoparticles such as CuO, NiO, and Cu/Ni hybrids, and we tested their antibacterial effectiveness against UTI bacterial strains [63]. In general, all strains tested were sensitive to all NPs shown in (Table 1 and Figure 8). Inhibition zones measured at 5 mg/mL for CuO, NiO, and Cu/Ni hybrids were 23 ± 1.53, 19 ± 1.11, and 25 ± 1.47 for *E. coli*, respectively. All test samples inhibited *P. aeuroginosa* and *P. vulgaris* in a dose-dependent manner; however, the highest zone of inhibition was observed against *P. aeuroginosa* (28 ± 1.22) and *P. vulgaris* (25 ± 1.73) for Cu/Ni hybrids, respectively. Plant- and bacterial-mediated NPs have good antimicrobial properties [64,65]. Furthermore, *E. coli* was the most susceptible strain to

antibiotic coated NPs, with significant zone of inhibition. However, all of the test bacterial spp were resistant to non-coated meropenem, imipenem, oxacillin, and Ciprofloxacin. It was observed that the activity of CuO, NiO, and Cu/Ni hybrids coated with antibiotics showed an increase in inhibition against *Proteus Vulgaris.*

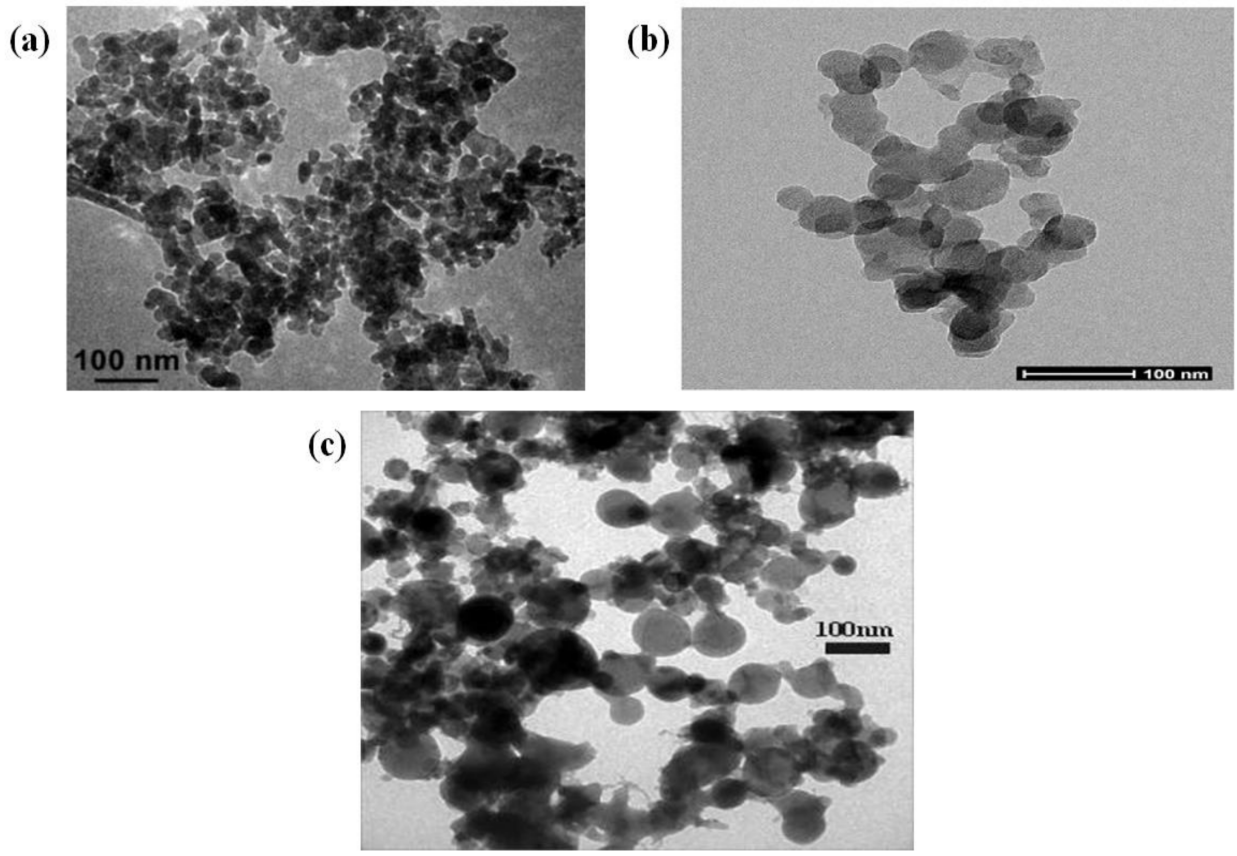

Figure 7. TEM micrograph of *Curcuma longa*: (**a**) CuO, (**b**) NiO and (**c**) Cu/Ni hybrids.

Table 1. Antibacterial activity of *Curcuma longa* CuO, NiO and Cu/Ni hybrids against UTI isolates.

Bacterial Strains	NPs	ZOI of NPs	Antibiotics	CLSI	ZOI of Non-coated Antibiotics	ZOI of Coated NPs	% Increased Potency of Coated NPs
Pseudomonas aurigenosa	CuO	11 ± 0.9	MEM	18	12 ± 1.1	18 ± 1.1	33.3
			IPM	22	10 ± 1.0	16 ± 1.2	27.2
			OX	17	09 ± 0.8	14 ± 0.5	29.5
			CIP	21	13 ± 0.7	19 ± 1.2	3
	NiO	20 ± 1.22	MEM	18	12 ± 1.1	24 ± 0.8	66.6
			IPM	22	10 ± 1.0	15 ± 1.0	22.7
			OX	17	09 ± 0.8	13 ± 0.6	23.6
			CIP	21	13 ± 0.7	22 ± 1.1	42.9
	Cu + Ni	28 ± 1.22	MEM	18	12 ± 1.1	17 ± 1.3	27.7
			IPM	22	10 ± 1.0	13 ± 0.5	13.6
			OX	17	09 ± 0.8	12 ± 0.6	17.7
			CIP	18	12 ± 1.1	18 ± 1.1	33.3

Table 1. *Cont.*

Bacterial Strains	NPs	ZOI of NPs	Antibiotics	CLSI	ZOI of Non-coated Antibiotics	ZOI of Coated NPs	% Increased Potency of Coated NPs
Proteus Vulgaris	CuO	18 ± 1.68	MEM	18	9 ± 0.5	17 ± 0.8	44.4
			IPM	22	11 ± 1.0	14 ± 1.5	13.6
			OX	17	8 ± 0.9	12 ± 1.2	23.6
			CIP	21	15 ± 1.23	21 ± 1.4	28.6
	NiO	23 ± 1.23	MEM	18	9 ± 0.5	20 ± 0.9	61.1
			IPM	22	11 ± 1.0	19 ± 1.0	36.4
			OX	17	8 ± 0.9	17 ± 1.1	53.0
			CIP	21	15 ± 1.23	20 ± 0.8	20.8
	Cu + Ni	25 ± 1.73	MEM	18	9 ± 0.5	17 ± 1.3	24.4
			IPM	22	11 ± 1.0	18 ± 0.5	31.8
			OX	17	8 ± 0.9	14 ± 0.7	35.4
			CIP	21	15 ± 1.23	17 ± 0.6	9.6
E. coli	CuO	23 ± 1.53	MEM	18	15 ± 0.7	20 ± 0.3	27.8
			IPM	22	13 ± 1.0	17 ± 1.1	18.3
			OX	17	10 ± 0.9	15 ± 0.8	29.4
			CIP	21	14 ± 1.2	19 ± 0.7	23.8
	NiO	19 ± 1.11	MEM	18	15 ± 0.7	18 ± 0.5	16.7
			IPM	22	13 ± 1.0	22 ± 1.2	41.0
			OX	17	10 ± 0.9	12 ± 0.3	11.8
			CIP	21	14 ± 1.2	20 ± 1.1	28.5
	Cu + Ni	25 ± 1.47	MEM	18	15 ± 0.7	19 ± 1.4	22.3
			IPM	22	13 ± 1.0	16 ± 0.9	13.7
			OX	17	10 ± 0.9	13 ± 0.6	17.7
			CIP	21	14 ± 1.2	22 ± 1.3	38.0

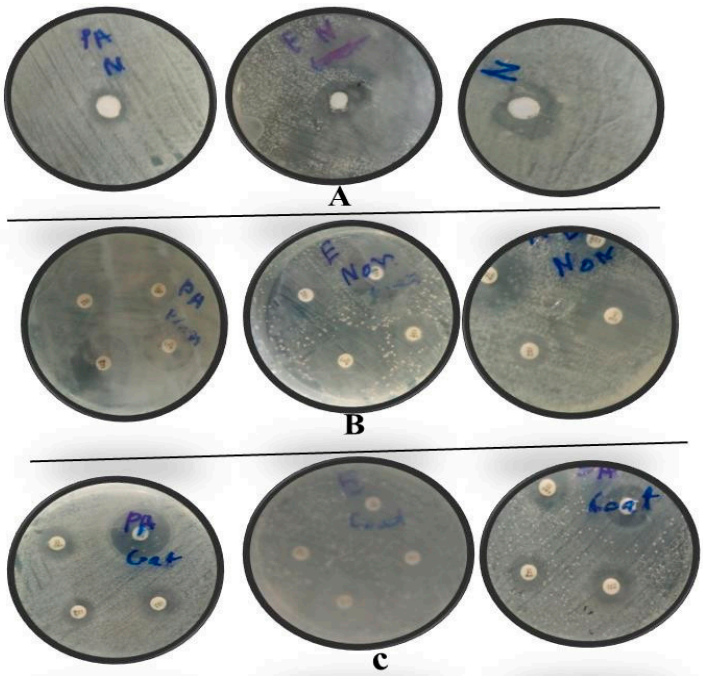

Figure 8. (**A**) Activity of Hybrid NPs, Copper NPs, Nickle NPs (**B**) Activity of antibiotics. (**C**) Activity of Hybrid NPs, Copper NPs, Nickle NPs Nanoparticles Coated with Antibiotics.

3.9. Anti-Leishmanial Assay

Leishmaniasis is a parasitic infection caused primarily by parasites of the genus Leishmania. It is a potentially fatal, non-contagious disease [66], and causes 50,000 deaths per year (WHO) [67]. The epidemic carries a high risk of uncontrolled spreading due to a lack of vectors and inefficient and inexpensive antibiotics. As shown in Figure 9a, dose-dependent cytotoxicity was observed with mortality rates of 60.5 ± 0.53 and 68.4 ± 0.59 for Cu/Ni hybrids; 53.2 ± 0.48 and 61.2 ± 0.44 for NiO-NPs; 49.1 ± 0.39 and 56.2 ± 0.45 for CuO-NPs at 400 µg/mL for promastigote and amastigotes, respectively. Moreover, the lowest value of 9.2 ± 0.19 for promastigote and 13.6 ± 0.21 for amastigote was shown for CuO-NPs. Our results were same with [68].

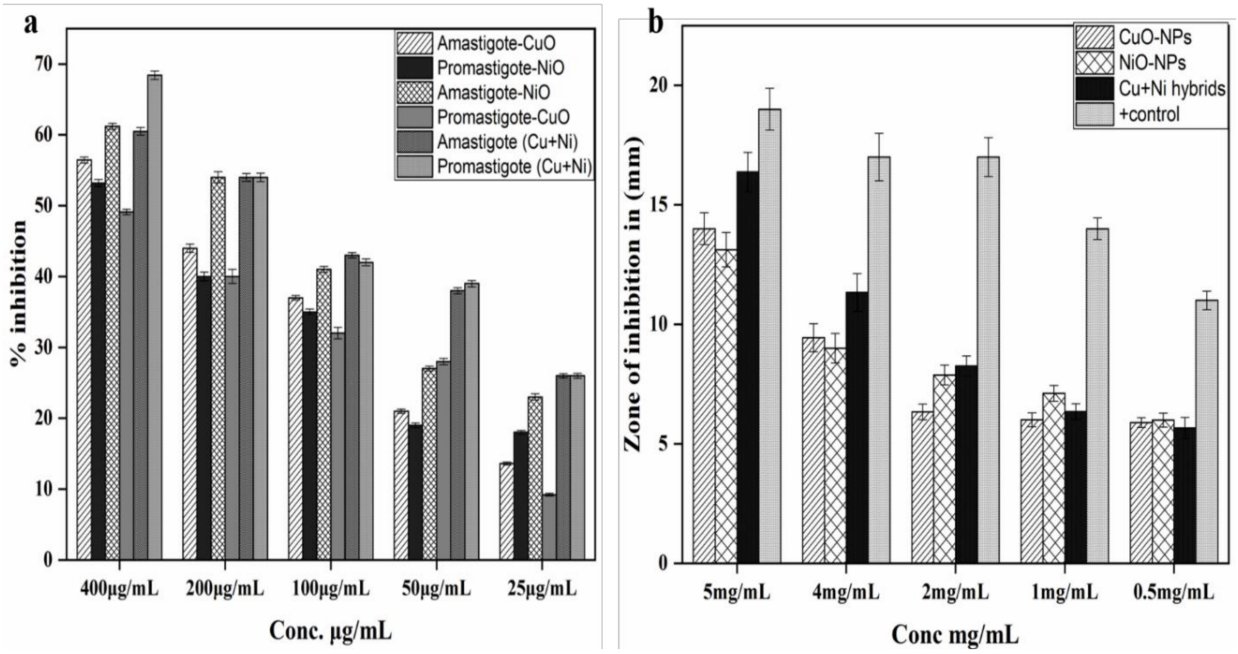

Figure 9. (**a**) Anti-leishmanial and (**b**) Protein kinase inhibition potential of synthesized NPs.

3.10. Protein Kinase Inhibition Assay

Protein kinase inhibitors play an important role in the treatment of cancer. Achieving inhibitor selectivity remains an important issue for researchers, so the synthesis of alternative compounds for research in chemical biology or new small molecules as drugs is still a choice of interest [69,70]. These enzymes phosphorylate serine-threonine and tyrosine amino acid residues, which have a key function in cellular proliferation, namely, differentiation and apoptosis [71]. The streptomyces 85E strain was used to examine the protein kinase inhibition potential of *C. longa* synthesized NPs. The results are indicated in Figure 9b. It was observed that Cu + Ni hybrids solution (5 mg/mL) displayed maximum zone of inhibition (16.37 ± 0.82) and (5.66 ± 0.44) at 0.5 mg/mL, respectively. All metallic NPs inhibited the streptomyces strain at in a concentration-dependent manner (Figure 9b). Overall, the results showed that all test samples acquired vital metabolites responsible for anti-cancerous potentials in *C. longa*. These results are strongly supported by a previous report [35,69].

3.11. Anti-Cancer Activity against HepG2 Cell Line

In recent years, plant derived compounds and nanomaterials have been viewed as powerful and helpful alternative sources for the treatment of hepatocellular carcinoma [72]. The chemo-preventive and less harmful nature of these compounds with effective anti-cancer potential provides a research hotspot for the treatment of cancer. However, due to certain issues like inadequate solubility, structural deformation and bioavailability they

target cancer sites very poorly [73,74]. We explored the potential and cytotoxicity of mediated NPs in *C. longa* extracts against human hepatocytes (HepG2 cells). Like antimicrobial activities, Cu/Ni hybrids showed a higher inhibition of 73.18 ± 2.42% toward the fresh HepG2 cell line owing to its unique morphological properties. IC50 value was calculated as 129.44 ± 2.29%. Doxorubicin was used as positive control and resulted in 97.38 ± 2.71% inhibition of HepG2 cells. On the other side, the cytotoxicity of CuO-NPs and NiO-NPs was 64.10 ± 1.91% and 47.55 ± 1.61%, respectively, and is shown in Table 2 and Figure 10. DMSO functioned as a negative control [75]. The cytotoxic effect of these materials involves three key mechanisms, including their dissolution into functional entities, formation of reactive oxygen species (ROS), and DNA damage [75–77]. Moreover, physical properties, surface chemistry, and dosage dictates the overall uptake, elimination, and anti-tumor properties of the test samples [77]. However, most of the available data about in vitro anti-hepatocarcinoma activity is related to nature and the presence of chemicals in plant extracts used as successful capping agents. Our findings thus complement and support previously reported studies [78]. The pronounced antitumor activity against the HepG2 cell line indicates the exciting potential of *C. longa*, and their extracts mediated oxide nanoparticles are promising anti-cancer agents.

Table 2. Anti-cancer potential of various synthesized metallic NPs against HepG2 cell line.

S. No	Test Samples	% Inhibition
1	CuO	64.10 ± 1.91
2	NiO	47.55 ± 1.61
3	Cu + Ni	73.18± 2.42
4	NTC	0.00
5	DMSO	3.71
6	Doxorubicin	97.38 ± 2.71

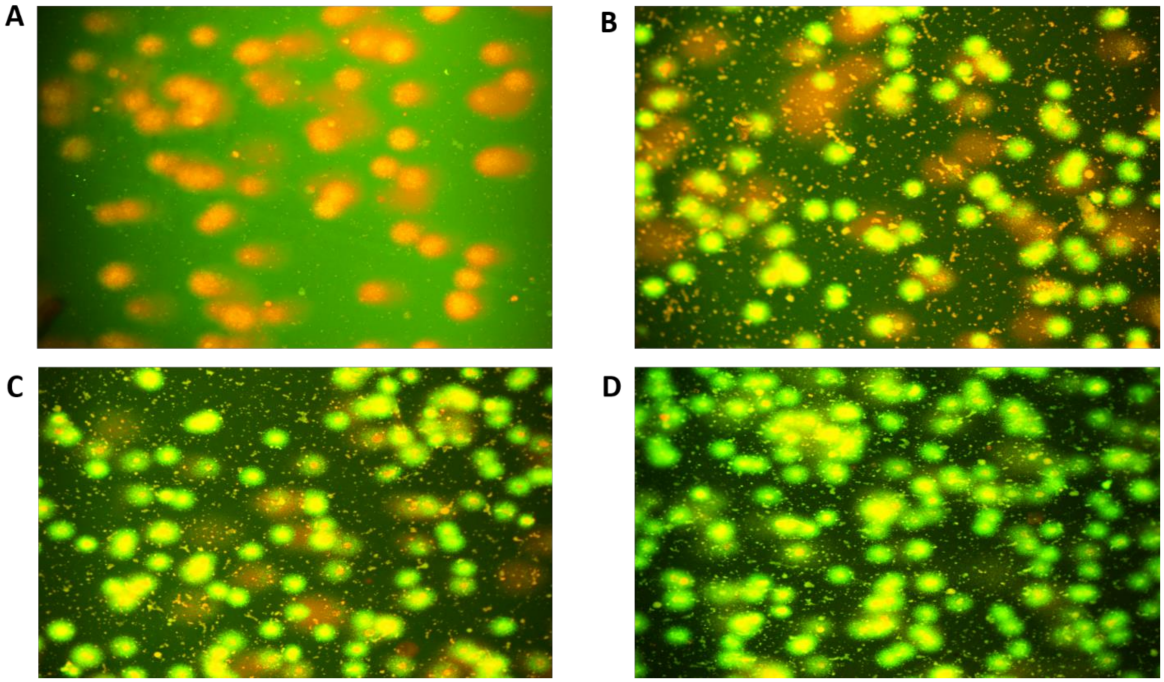

Figure 10. (**A**) Doxorubicin as positive control, (**B**) Hybrid NPs against cell lines, (**C**) Copper NPs against cell lines, (**D**) Nickel NPs against cell lines.

3.12. Anti-Diabetic Activity

Diabetes mellitus is a metabolic condition predominantly described by persistent hyperglycemia attributed to decreased insulin output or body cell insensitivity to insulin already produced [79,80]. The elimination of postprandial hyperglycemia, which can be accomplished through inhibition of alpha amylase and alpha glucosidase, the two most common carbohydrate hydrolyzing enzymes in the digestive tract, is one successful therapeutic technique for treating DM (Diabetes mellitus) [79]. As shown in Figure 11, a significant inhibition percentage for α-amylase (CuO-NPs: 52.35 ± 0.76, NiO-NPs: 68.1 ± 0.93 and Cu + Ni hybrids: 74.23 ± 0.42) as well as for α-glucosidase (CuO-NPs: 39.25 ± 0.18, NiO-NPs: 52.35 ± 1.32 and Cu + Ni hybrids 62.32 ± 0.48) was calculated respectively at 400 µg/mL. The same results were also observed by [81,82].

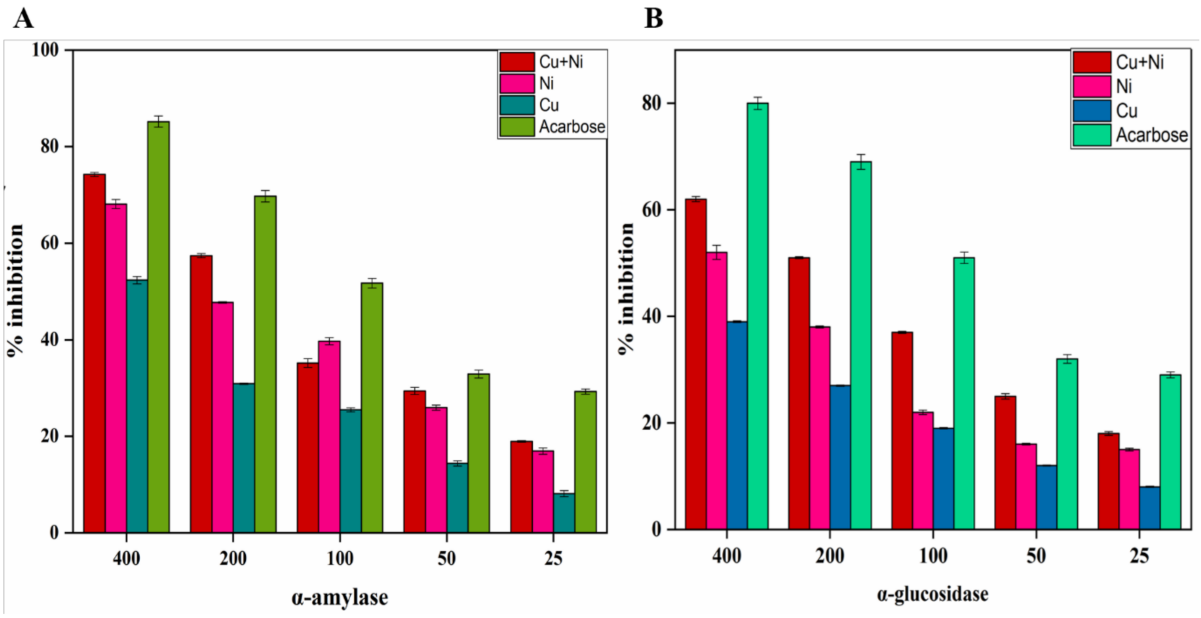

Figure 11. Percentage of inhibition activity of *Curcuma longa* synthesized NPs against (**A**) α–amylase and (**B**) α–glucosidase enzymes.

3.13. In Vitro AChE and BChE Inhibition Assays

The diagnosis of Alzheimer's is a progressive neurodegenerative disorder that results in 60%–80% of all dementia cases worldwide. The condition is characterized by a slow regression of cognitive abilities such as memory, space function and visuality, personality, and vocabulary. The incidence of disease occurrence in the United States alone is alarming and a person develops Alzheimer's disease in 65 year of age [83]. The cholinesterase inhibitors for patients with any level of AD are now available for AD therapy. For efficient inhibition of cholinesterase enzymes, various synthetic and natural substances have been published. In the synapses or neuro-muscular junctions of tissues, the enzymes act by catalyzing acetylcholine hydrolysis (neurotransmitter) into choline and acetic acid. Reduced acetyl choline levels lead to AD development. The inhibition reaction of two enzymes Acetylcholinesterase (AChE) and butrylcholineterase were tested at varying consistencies of NPs [84]. Surprisingly, both esterases' inhibition reaction were dose dependent. NiO-NPs were mostly active at 400 µg/mL, which resulted in 71.49 ± 2.44% inhibition of AChE and 63.45 ± 1.39% for BChE, followed by Cu + Ni hybrids, which resulted in 67.71 ± 2.92% for AChE and 61.73 ± 2.11% for BChE. A lower inhibition response of AChE 18.43 ± 0.41% and BChE 21.20% ± 0.49 at 25 µg/mL was observed by CuO-NPs. As shown by the values in Table 3, NPs is found to be highly active against both enzymes. Our findings are consistent with previous research [85,86].

Table 3. In vitro AChE and BChE inhibition potential of synthesized metallic NPs.

Enzymes	NPs	25 µg/mL	50 µg/mL	100 µg/mL	200 µg/mL	400 µg/mL
AChE	CuO	18.43 ± 0.41	24.92 ± 0.67	32.81 ± 0.61	44.19 ± 1.41	63.39 ± 2.28
	NiO	23.20 ± 0.67	33.19 ± 1.13	47.28 ± 1.19	61.29 ± 1.39	71.49 ± 2.44
	Cu + Ni	21.82 ± 0.41	27.82 ± 0.44	39.49 ± 0.92	52.29 ± 1.19	67.71 ± 2.92
BChE	CuO	21.20 ± 0.49	29.92 ± 0.49	37.27 ± 0.93	42.22 ± 1.10	53.28 ± 2.19
	NiO	27.54 ± 0.39	39.22 ± 0.44	46.44 ± 0.73	58.92 ± 1.28	63.45 ± 1.39
	Cu + Ni	24.31 ± 0.43	29.39 ± 0.53	37.28 ± 0.57	46.67 ± 1.22	61.73 ± 2.11

3.14. Antioxidant Assays

Environmental stress is attributed to the change in plant metabolic pathways, which results in reactive oxygen species (ROS) destroying membrane lipids, plant cells, DNA, and proteins [87]. Plants produce numerous metabolic compounds such as flavonoids, terpenoids, and phenolics that act as protective mechanisms, while these phytochemicals are primarily involved in the stabilization and capping of respective nanoparticles [88,89]. To evaluate the in vitro antioxidant potential of plant-synthesized NPs, four separate assays were performed: total antioxidant capacity (TAC); total reduction power (TRP); ABTS; DPPH-free radical scavenging assays (FRSA). The outcomes are summarized in Table 4. The total antioxidant potential (TAC) was tested using a phosphomolybdenum-based technique that relies on an antioxidant mediator reducing Mo (VI) to Mo (V), resulting in the development of a complex of phosphate-molybdate, which is distinguished by its green color [90]. The highest antioxidants capacity in terms of ascorbic acid equivalents was observed as 65.1 ± 0.83 µgAAE/mg for Cu + Ni NPs; 58.39 ± 0.62 µgAAE/mg for Ni NPs; and 52.2 ± 0.31 µgAAE/mg for Cu NPs, respectively, at 400 µg/mL. The complete reducing power estimate (TRP) assay was used to boost TAC activity. The assay was focused on the tested sample, converting Fe^{+3} to Fe^{+2} ion if it had redox power [91]. The highest TRP was noted as 56.4 ± 0.83 for Cu + Ni NPs; 51.5 ± 0.71 for Ni NPs; and 43.2 ± 0.49 for Cu NPs, respectively. ABTS and DPPH free radical scavenging tests were also conducted to provide evidence for TAC and TRP findings. Furthermore, free scavenging tests were performed to support TAC and TRP findings. DPPH is a neutral free radical which is reduced in the form of yellowish picrylhydrazine molecules by accepting hydrogen and/or the electron in the donor [92,93]. The basis of these spectrophotometric methods is the quenching of stable color in DPPH and ABTS radicals, showing the antioxidant specimen's scavenging capabilities. The analysis showed that all research samples had an outstanding free radical scavenging activity, as summarized in Table 4. The highest DPPH and ABTS free radical scavenging activity at 400 µg/mL was noted as 76.3 ± 0.28% and 80.1 ± 0.28 TEAC for Cu + Ni NPs, respectively. Obtained results were in correspondence with [63,94].

3.15. In-Vitro Biocompatibility Studies

Nanoparticles have been studied for hemolysis against human red blood cells in order to assess the effects toxicological potential. Freshly extracted RBCs and various NP formulations (25–400 µg/mL) have been co-incubated in an extracellular buffer solution in the testing. The theory is based on the romping of RBCs that can be quantified by spectrophotometer with hemoglobin releases in the medium at 405 nm. This can only be induced by the cell rupture potential of the tested specimen. Hemolysis is considered non-hemolytic by ASTM (American Society of Testing and Materials) standards when 2 to 5% hemolytic by 2%, and when hemolytic by 5% [94], as seen in Table 5. Except at the greatest stock concentration, no eminent hemolytic activity was seen at all in NPs showing exceptional hemocompatibility. For biomedical applications, the biocompatibility of the nanomaterial (ENMs) developed is an integral prerequisite. Particles showed great hemocompatibility, so no hemolytic activity was detected, even at the maximum concentration of 400 µg/mL. The bio-safe character of the particles is thus reaffirmed by our findings and paves the

way for the long-summary NPs that are sent for treatment. Our findings are in line with previous studies [95,96].

Table 4. Antioxidant potential of *Curcuma longa* CuO, NiO and Cu + Ni hybrids.

NPs	Conc (µg/mL)	TAC (µg AAE/mg)	TRP (µg AAE/mg)	ABTS (CTEAC)	DPPH (%FRSA)
Cu + Ni	400	65.1 ± 0.83	56.41 ± 0.83	80.12 ± 0.28	76.3 ± 0.28
	200	34.37 ± 0.27	49.51 ± 0.87	49.63 ± 0.39	42.1 ± 0.71
	100	29.86 ± 0.72	32.23 ± 0.26	33.64 ± 0.56	35.69 ± 0.32
	50	17.29 ± 0.76	25.76 ± 0.58	29.47 ± 0.26	20.45 ± 0.98
	25	12.16 ± 0.25	22.41 ± 0.36	13.39 ± 0.15	16.19 ± 0.48
NiO	400	58.39 ± 0.62	51.52 ± 0.71	73.14 ± 0.38	69.4 ± 0.12
	200	33.37 ± 0.27	42.6 ± 0.18	51.63 ± 0.98	31.9 ± 0.73
	100	21.47 ± 0.52	34.29 ± 0.67	42.64 ± 0.56	27.25 ± 0.59
	50	16.29 ± 0.47	27.16 ± 0.52	34.47 ± 0.16	16.38 ± 0.18
	25	11.21 ± 0.73	20.16 ± 0.51	19.39 ± 0.15	12.89 ± 0.64
CuO	400	52.2 ± 0.31	43.23 ± 0.49	68.63 ± o.93	60.53 ± 0.67
	200	44.31 ± 0.73	38.71 ± 0.27	52.64 ± 0.63	41.36 ± 0.77
	100	33.86 ± 0.81	24.86 ± 0.72	41.33 ± 0.31	33.39 ± 0.16
	50	19.73 ± 0.10	14.93 ± 0.61	32.86 ± 0.62	25.52 ± 0.48
	25	12.30 ± 0.12	8.21 ± 0.41	19.14 ± 0.51	14.93 ± 0.28

Table 5. Percentage of hemolytic activity of *Curcuma longa* CuO, NiO and Cu + Ni hybrids.

Conc. (µg/mL)	% Hemolysis of NPs		
	Cu + Ni	Ni	Cu
400	3.42 ± 0.19	1.42 ± 0.10	1.53 ± 0.50
200	2.19 ± 0.14	1.50 ± 0.41	1.90 ± 0.13
100	1.10 ± 0.13	O.84 ± 0.50	0.63 ± 0.90
50	0.40 ± 0.10	0.60 ± 0.21	0.20 ± 0.13

4. Conclusions

A facile and nonhazardous synthesis protocol of CuO-NPs, NiO-NPs, and Cu/Ni hybrids NPs using an aqueous extract of *Curcuma longa*, a potential reducing and stabilizing source, has been described. The FTIR analysis confirmed the successful capping of naturally-occurring phytoconstituents of the plant extract such as phenols, polysaccharides, and guanine. The morphological examination using SEM and TEM showed the mean size of the NPs. The NPs were screened for a variety of biological applications, including bactericidal activity against urinary tract infection (UTI) isolates, leishmaniasis, anti-diabetic, antioxidant, anti-cancer, and biocompatibility studies. Our study revealed that CuO, NiO, and its hybrid NPs were highly active against multidrug-resistant UTI isolates as compared to conventional antibiotics. Both NPs, particularly hybrid NPs, also showed significant anti-leishmanial and cytotoxic activities against HepG2 cell lines, respectively. Furthermore, the NPs significantly inhibited α-amylase and α-glucosidase, the key enzymes involved in the onset of diabetes mellitus (DM). Moreover, the NPs were found to be excellent antioxidant and anti-Alzheimer's agents. Last but not least, the nonhazardous and biocompatible nature makes the *Curcuma longa* synthesized NPs a green and inexpensive potential alternative for biomedical and clinical applications.

Author Contributions: Conceptualization, S.F. and H.J.; methodology, N.S.A.-R. and A.; software, N.S.A.-R. and M.R.; validation, Z.A., Z.H.; formal analysis, M.N.U., M.I. and N.B.; writing—original draft preparation, H.J., S.F. and N.S.A.-R. writing—review and editing, H.J.; supervision, S.A.S. and S.S. All authors have read and agreed to the published version of the manuscript.

Funding: This research received no external funding.

Institutional Review Board Statement: Not applicable.

Informed Consent Statement: Not applicable.

Data Availability Statement: All data is available in the manuscript.

Conflicts of Interest: The authors declare no conflict of interest.

References

1. Ramsden, J. *Nanotechnology: An Introduction*; William Andrew: Norwich, NY, USA, 2016.
2. Albrecht, M.A.; Evans, C.W.; Raston, C.L. Green chemistry and the health implications of nanoparticles. *Green Chem.* **2006**, *8*, 417–432. [CrossRef]
3. Al-Radadi, N.S.; Adam, S.I. Green biosynthesis of Pt-nanoparticles from Anbara fruits: Toxic and protective effects on CCl4 induced hepatotoxicity in Wister rats. *Arab. J. Chem.* **2020**, *13*, 4386–4403. [CrossRef]
4. Al-Radadi, N.S. Artichoke (*Cynara scolymus* L.) Mediated Rapid Analysis of Silver Nanoparticles and Their Utilisation on the Cancer Cell Treatments. *J. Comput. Nanosci.* **2018**, *15*, 1818–1829. [CrossRef]
5. Al-Radadi, N.S. Green synthesis of platinum nanoparticles using Saudi's Dates extract and their usage on the cancer cell treatment. *Arab. J. Chem.* **2019**, *12*, 330–349. [CrossRef]
6. Herlekar, M.; Barve, S.; Kumar, R. Plant-mediated green synthesis of iron nanoparticles. *J. Nanoparticles* **2014**, *2014*, 140614. [CrossRef]
7. Simonis, F.; Schilthuizen, S. *Nanotechnology*; Innovation Opportunities for Tomorrow's Defence; TNO: Eindhoven, The Netherlands, 2006.
8. Al-Radadi, N.S.; Al-Youbi, A.N. One-Step Synthesis of Au Nano-Assemblies and Study of Their Anticancer Activities. *J. Comput. Theor. Nanosci.* **2018**, *15*, 1861–1870. [CrossRef]
9. Al-Radadi, N.S.; Al-Youbi, A.N. Environmentally-Safe Synthesis of Gold and SilverNano-Particles with AL-Madinah Barni Fruit and Their Applications in the Cancer Cell Treatments. *J. Comput. Theor. Nanosci.* **2018**, *15*, 1853–1860. [CrossRef]
10. Ullah, R.; Shah, S.; Muhammad, Z.; Shah, S.A.; Faisal, S.; Khattak, U.; ul Haq, T.; Akbar, M.T. In vitro and in vivo applications of Euphorbia wallichii shoot extract-mediated gold nanospheres. *Green Process. Synth.* **2021**, *10*, 101–111. [CrossRef]
11. Duan, H.; Wang, D.; Li, Y. Green chemistry for nanoparticle synthesis. *Chem. Soc. Rev.* **2015**, *44*, 5778–5792. [CrossRef]
12. Bala, N.; Saha, S.; Chakraborty, M.; Maiti, M.; Das, S.; Basu, R.; Nandy, P. Green synthesis of zinc oxide nanoparticles using Hibiscus subdariffa leaf extract: Effect of temperature on synthesis, anti-bacterial activity and anti-diabetic activity. *RSC Adv.* **2015**, *5*, 4993–5003. [CrossRef]
13. Hasan, S. A review on nanoparticles: Their synthesis and types. *Res. J. Recent Sci.* **2015**, *2277*, 2502.
14. Barzinjy, A.A.; Hamad, S.M.; Aydın, S.; Ahmed, M.H.; Hussain, F.H. Green and eco-friendly synthesis of Nickel oxide nanoparticles and its photocatalytic activity for methyl orange degradation. *J. Mater. Sci. Mater. Electron.* **2020**, *31*, 11303–11316. [CrossRef]
15. Shah, R.; Shah, S.A.; Shah, S.; Faisal, S.; Ullah, F. Green Synthesis and Antibacterial Activity of Gold Nanoparticles of Digera muricata. *Indian J. Pharm. Sci.* **2020**, *82*, 374–378. [CrossRef]
16. Ren, G.; Hu, D.; Cheng, E.W.; Vargas-Reus, M.A.; Reip, P.; Allaker, R.P. Characterisation of copper oxide nanoparticles for antimicrobial applications. *Int. J. Antimicrob. Agents* **2009**, *33*, 587–590. [CrossRef] [PubMed]
17. Verma, N.; Kumar, N. Synthesis and biomedical applications of copper oxide nanoparticles: An expanding horizon. *Acs Biomater. Sci. Eng.* **2019**, *5*, 1170–1188. [CrossRef]
18. Imran Din, M.; Rani, A. Recent advances in the synthesis and stabilization of nickel and nickel oxide nanoparticles: A green adeptness. *Int. J. Anal. Chem.* **2016**, *2016*, 1–14. [CrossRef]
19. Mishra, P.K.; Mishra, H.; Ekielski, A.; Talegaonkar, S.; Vaidya, B. Zinc oxide nanoparticles: A promising nanomaterial for biomedical applications. *Drug Discov. Today* **2017**, *22*, 1825–1834. [CrossRef] [PubMed]
20. Nagajyothi, P.; Cha, S.J.; Yang, I.J.; Sreekanth, T.; Kim, K.J.; Shin, H.M. Antioxidant and anti-inflammatory activities of zinc oxide nanoparticles synthesized using Polygala tenuifolia root extract. *J. Photochem. Photobiol. B Biol.* **2015**, *146*, 10–17. [CrossRef] [PubMed]
21. Cai, X.; Luo, Y.; Zhang, W.; Du, D.; Lin, Y. pH-Sensitive ZnO quantum dots–doxorubicin nanoparticles for lung cancer targeted drug delivery. *ACS Appl. Mater. Interfaces* **2016**, *8*, 22442–22450. [CrossRef]
22. Gutha, Y.; Pathak, J.L.; Zhang, W.; Zhang, Y.; Jiao, X. Antibacterial and wound healing properties of chitosan/poly (vinyl alcohol)/zinc oxide beads (CS/PVA/ZnO). *Int. J. Biol. Macromol.* **2017**, *103*, 234–241. [CrossRef]

23. Lai, L.; Zhao, C.; Su, M.; Li, X.; Liu, X.; Jiang, H.; Amatore, C.; Wang, X. In vivo target bio-imaging of Alzheimer's disease by fluorescent zinc oxide nanoclusters. *Biomater. Sci.* **2016**, *4*, 1085–1091. [CrossRef] [PubMed]
24. Witkin, J.M.; Li, X. Curcumin, an active constiuent of the ancient medicinal herb Curcuma longa L.: Some uses and the establishment and biological basis of medical efficacy. *CNS Neurol. Disord. Drug* **2013**, *12*, 487–497. [CrossRef] [PubMed]
25. Al-Radadi, N.S. Green Biosynthesis of Flaxseed Gold Nanoparticles(Au-NPs) as Potent Anti-cancer Agent Against Breast Cancer Cells. *J. Saudi Chem. Soc.* **2021**, *25*, 101243. [CrossRef]
26. Radadi, N.S. Facile one-step green synthesis of gold nanoparticles (AuNp) using licorice root extract: Antimicrobial and anticancer study against HepG2 cell line. *Arab. J. Chem.* **2021**, *14*, 102956.
27. Damalas, C.A. Potential uses of turmeric (*Curcuma longa*) products as alternative means of pest management in crop production. *Plant. Omics* **2011**, *4*, 136–141.
28. Padil, V.V.T.; Černík, M. Green synthesis of copper oxide nanoparticles using gum karaya as a biotemplate and their antibacterial application. *Int. J. Nanomed.* **2013**, *8*, 889.
29. Ezhilarasi, A.A.; Vijaya, J.J.; Kaviyarasu, K.; Zhang, X.; Kennedy, L.J. Green synthesis of nickel oxide nanoparticles using Solanum trilobatum extract for cytotoxicity, antibacterial and photocatalytic studies. *Surf. Interfaces* **2020**, *20*, 100553. [CrossRef]
30. Ismail, M.; Khan, M.; Khan, S.B.; Khan, M.A.; Akhtar, K.; Asiri, A.M. Green synthesis of plant supported CuAg and CuNi bimetallic nanoparticles in the reduction of nitrophenols and organic dyes for water treatment. *J. Mol. Liq.* **2018**, *260*, 78–91. [CrossRef]
31. Holzwarth, U.; Gibson, N. The Scherrer equation versus the Debye-Scherrer equation. *Nat. Nanotechnol.* **2011**, *6*, 534. [CrossRef]
32. Barzinjy, A.; Mustafa, S.; Ismael, H. Characterization of ZnO NPs prepared from green synthesis using Euphorbia Petiolata leaves. *EAJSE* **2019**, *4*, 74–83.
33. Shah, M.; Nawaz, S.; Jan, H.; Uddin, N.; Ali, A.; Anjum, S.; Giglioli-Guivarc'h, N.; Hano, C.; Abbasi, B.H. Synthesis of bio-mediated silver nanoparticles from Silybum marianum and their biological and clinical activities. *Mater. Sci. Eng. C* **2020**, *112*, 110889. [CrossRef]
34. Imran, M.; Jan, H.; Faisal, S.; Shah, S.A.; Shah, S.; Khan, M.N.; Syed, S. In vitro Examination of Anti-parasitic, An-ti-Alzheimer, Insecticidal and Cytotoxic Potential of Ajuga Bracteosa Wallich Leaves Extracts. *Saudi J. Biol. Sci.* **2021**, *28*, 3031–3036. [CrossRef]
35. Jan, H.; Khan, M.A.; Usman, H.; Shah, M.; Ansir, R.; Faisal, S.; Ullah, N.; Rahman, L. The Aquilegia pubiflora (*Himalayan columbine*) mediated synthesis of nanoceria for diverse biomedical applications. *RSC Adv.* **2020**, *10*, 19219–19231. [CrossRef]
36. Faisal, S.; Shah, S.A.; Shah, S.; Akbar, M.T.; Jan, F.; Haq, I.; Baber, M.E.; Aman, K.; Zahir, F.; Bobi, F.; et al. In Vitro Biomedical and Photo-Catalytic Application of Bio-Inspired Zingiber officinale Mediated Silver Nanoparticles. *J. Biomed. Nanotechnol.* **2020**, *16*, 492–504. [CrossRef] [PubMed]
37. Faisal, S.; Jan, H.; Shah, S.A.; Khan, A.; Akbar, M.T.; Rizwan, M.; Jan, F.; Wajidullah; Akhtar, N.; Khattak, A.; et al. Green Synthesis of Zinc Oxide (ZnO) Nanoparticles Using Aqueous2 Fruit Extracts of Myristica fragrans: Their Characterizations and Biological and Environmental Applications. *ACS Omega* **2021**, *6*, 9709–9722. [CrossRef]
38. Usman, H.; Ullah, M.A.; Jan, H.; Siddiquah, A.; Drouet, S.; Anjum, S.; Giglioli-Guviarc'h, N.; Hano, C.; Abbasi, B.H. Interactive Effects of Wide-Spectrum Monochromatic Lights on Phytochemical Production, Antioxidant and Biological Activities of Solanum xanthocarpum Callus Cultures. *Molecules* **2020**, *25*, 2201. [CrossRef]
39. Ellman, G.L.; Courtney, K.D.; Andres, V., Jr.; Featherstone, R.M. A new and rapid colorimetric determination of acetylcholinesterase activity. *Biochem. Pharm.* **1961**, *7*, 88–95. [CrossRef]
40. Faisal, S.; Jan, H.; Shah, S.A.; Shah, S.; Zaman, N.; Hussain, Z.N.; Uddin, M.N.; Bibi, N.; Khattak, A.; Khan, W.; et al. Bio-Catalytic Activity of Novel Mentha arvensis Intervened Biocompatible Magnesium Oxide Nanomaterials. *Catalysts* **2021**, *11*, 780. [CrossRef]
41. Nazir, S.; Jan, H.; Tungmunnithum, D.; Drouet, S.; Zia, M.; Hano, C.; Abbasi, B.H. Callus Culture of Thai Basil Is an Effective Biological System for the Production of Antioxidants. *Molecules* **2020**, *25*, 4859. [CrossRef]
42. Abdel-Aziz, H.M.; Rizwan, M. Chemically synthesized silver nanoparticles induced physio-chemical and chloroplast ultrastructural changes in broad bean seedlings. *Chemosphere* **2019**, *235*, 1066–1072. [CrossRef]
43. Faisal, S.; Khan, M.A.; Jan, H.; Shah, S.A.; Shah, S.; Rizwan, M.; Ullah, W.; Akbar, M.T. Edible mushroom (*Flammulina velutipes*) as biosource for silver nanoparticles: From synthesis to diverse biomedical and environmental applications. *Nanotechnology* **2020**, *32*, 065101. [CrossRef] [PubMed]
44. Nisar, T.; Iqbal, M.; Raza, A.; Safdar, M.; Iftikhar, F.; Waheed, M. Turmeric: A promising spice for phytochemical and antimicrobial activities. *Am. EurJ. Agric. Environ. Sci.* **2015**, *15*, 1278–1288.
45. Himesh, S.; Sharan, P.S.; Mishra, K. Qualitative and quantitative profile of curcumin from ethanolic extract of *Curcuma longa*. *Int. Res. J. Pharm.* **2011**, *2*, 180–184.
46. Shah, S.; Shah, S.A.; Faisal, S.; Khan, A.; Ullah, R.; Ali, N.; Bilal, M. Engineering novel gold nanoparticles using Sageretia thea leaf extract and evaluation of their biological activities. *J. Nanostructure Chem.* **2021**, 1–12. [CrossRef]
47. Sabouri, Z.; Akbari, A.; Hosseini, H.A.; Darroudi, M. Facile green synthesis of NiO nanoparticles and investigation of dye degradation and cytotoxicity effects. *J. Mol. Struct.* **2018**, *1173*, 931–936. [CrossRef]
48. Nasrollahzadeh, M.; Sajjadi, M.; Komber, H.; Khonakdar, H.A.; Sajadi, S.M. In situ green synthesis of Cu-Ni bimetallic nanoparticles supported on reduced graphene oxide as an effective and recyclable catalyst for the synthesis of N-benzyl-N-aryl-5-amino-1H-tetrazoles. *Appl. Organomet. Chem.* **2019**, *33*, e4938. [CrossRef]

49. Guilger-Casagrande, M.; de Lima, R. Synthesis of Silver Nanoparticles Mediated by Fungi: A Review. *Front. Bioeng. Biotechnol.* **2019**, *7*, 287. [CrossRef]
50. Berestova, T.V.; Khursan, S.L.; Mustafin, A.G. Experimental and theoretical substantiation of differences of geometric isomers of copper (II) α-amino acid chelates in ATR-FTIR spectra. *Spectrochim. Acta Part A Mol. Biomol. Spectrosc.* **2020**, *229*, 117950. [CrossRef]
51. Zhang, H.; Han, B.; Meng, J. Photocatalytic Activity of Dye Sensitized Hematite Nanoparticles on Cenospheres. *J. Nanosci. Nanotechnol.* **2016**, *16*, 12433–12443. [CrossRef]
52. Mohamed, E.A. Green synthesis of copper & copper oxide nanoparticles using the extract of seedless dates. *Heliyon* **2020**, *6*, e03123.
53. He, N.; Yang, X.; Shi, L.; Yang, X.; Lu, Y.; Tong, G.; Wu, W. Chemical conversion of Cu_2O/PPy core-shell nanowires (CSNWs): A surface/interface adjustment method for high-quality Cu/Fe/C and Cu/Fe_3O_4/C CSNWs with superior microwave absorption capabilities. *Carbon* **2020**, *166*, 205–217. [CrossRef]
54. Jeevanandam, J.; San Chan, Y.; Wong, Y.J.; Hii, Y.S. *Biogenic Synthesis of Magnesium Oxide Nanoparticles Using Aloe Barbadensis Leaf Latex Extract*; IOP Conference Series Materials Science and Engineering, 2020; IOP Publishing: Bristol, UK, 2020.
55. Wu, M.; Wu, X.; Zhang, L.; Abdelhafiz, A.; Chang, I.; Qu, C.; Jiang, Y.; Zeng, J.; Alamgir, F. Cu@ Pt catalysts prepared by galvanic replacement of polyhedral copper nanoparticles for polymer electrolyte membrane fuel cells. *Electrochim. Acta* **2019**, *306*, 167–174. [CrossRef]
56. Song, H.-J.; Jia, X.-H.; Yang, X.-F.; Tang, H.; Li, Y.; Su, Y.-T. Controllable synthesis of monodisperse polyhedral nickel nanocrystals. *CrystEngComm* **2012**, *14*, 405–410. [CrossRef]
57. Suman, T.; Rajasree, S.R.; Kanchana, A.; Elizabeth, S.B. Biosynthesis, characterization and cytotoxic effect of plant mediated silver nanoparticles using Morinda citrifolia root extract. *Colloids Surf. B Biointerfaces* **2013**, *106*, 74–78. [CrossRef] [PubMed]
58. Michael, C.A.; Dominey-Howes, D.; Labbate, M. The antimicrobial resistance crisis: Causes, consequences, and management. *Front. Public Health* **2014**, *2*, 145. [CrossRef]
59. Romero, C.D.; Chopin, S.F.; Buck, G.; Martinez, E.; Garcia, M.; Bixby, L. Antibacterial properties of common herbal remedies of the southwest. *J. Ethnopharmacol.* **2005**, *99*, 253–257. [CrossRef] [PubMed]
60. Boucher, H.W.; Talbot, G.H.; Bradley, J.S.; Edwards, J.E.; Gilbert, D.; Rice, L.B.; Scheld, M.; Spellberg, B.; Bartlett, J. Bad bugs, no drugs: No ESKAPE! An update from the Infectious Diseases Society of America. *Clin. Infect. Dis.* **2009**, *48*, 1–12. [CrossRef]
61. Talbot, G.H.; Bradley, J.; Edwards Jr, J.E.; Gilbert, D.; Scheld, M.; Bartlett, J.G. Bad bugs need drugs: An update on the development pipeline from the Antimicrobial Availability Task Force of the Infectious Diseases Society of America. *Clin. Infect. Dis.* **2006**, *42*, 657–668. [CrossRef]
62. Kuppusamy, P.; Yusoff, M.M.; Maniam, G.P.; Govindan, N. Biosynthesis of metallic nanoparticles using plant derivatives and their new avenues in pharmacological applications—An updated report. *Saudi Pharm. J.* **2016**, *24*, 473–484. [CrossRef]
63. Hassan, N.; Shah, H.; Junaid, M.; Shah, S.A.; Faisal, S. Antimicrobial Activity and Biomedical Application of Sambucus wighfiana Phenolic Extract against Gram Positive and Gram-Negative Strains of Bacteria. *J. Biomed. Sci.* **2020**, *9*, 12.
64. Argueta-Figueroa, L.; Morales-Luckie, R.A.; Scougall-Vilchis, R.J.; Olea-Mejía, O.F. Synthesis, characterization and antibacterial activity of copper, nickel and bimetallic Cu–Ni nanoparticles for potential use in dental materials. *Prog. Nat. Sci. Mater. Int.* **2014**, *24*, 321–328. [CrossRef]
65. Karunakaran, G.; Jagathambal, M.; Gusev, A.; Van Minh, N.; Kolesnikov, E.; Mandal, A.R.; Kuznetsov, D. *Nitrobacter* sp. extract mediated biosynthesis of Ag_2O NPs with excellent antioxidant and antibacterial potential for biomedical application. *IET Nanobiotechnology* **2016**, *10*, 425–430. [CrossRef] [PubMed]
66. Ribeiro, J.B.P.; Miranda-Vilela, A.L.; Graziani, D.; de Aguiar Gomes, M.R.; Amorim, A.A.S.; Garcia, R.D.; de Souza Filho, J.; Tedesco, A.C.; Primo, F.L.; Moreira, J.R. Evaluation of the efficacy of systemic miltefosine associated with photodynamic therapy with liposomal chloroaluminium phthalocyanine in the treatment of cutaneous leishmaniasis caused by *Leishmania* (L.) *amazonensis* in C57BL/6 mice. *Photodiagnosis Photodyn.* **2016**, *13*, 282–290. [CrossRef] [PubMed]
67. Akbari, M.; Oryan, A.; Hatam, G. Application of nanotechnology in treatment of leishmaniasis: A Review. *Acta Trop.* **2017**, *172*, 86–90. [CrossRef]
68. Jebali, A.; Kazemi, B. Nano-based antileishmanial agents: A toxicological study on nanoparticles for future treatment of cutaneous leishmaniasis. *Toxicol. Vitr.* **2013**, *27*, 1896–1904. [CrossRef]
69. Jan, H.; Shah, M.; Usman, H.; Khan, A.; Muhammad, Z.; Hano, C.; Abbasi, B.H. Biogenic Synthesis and Characterization of Antimicrobial and Anti-parasitic Zinc Oxide (ZnO) Nanoparticles using Aqueous Extracts of the Himalayan Columbine (*Aquilegia pubiflora*). *Front. Mater.* **2020**, *7*, 249. [CrossRef]
70. Ferguson, F.M.; Gray, N.S. Kinase inhibitors: The road ahead. *Nat. Rev. Drug Discov.* **2018**, *17*, 353. [CrossRef] [PubMed]
71. Bain, J.; Plater, L.; Elliott, M.; Shpiro, N.; Hastie, C.J.; Mclauchlan, H.; Klevernic, I.; Arthur, J.S.C.; Alessi, D.R.; Cohen, P. The selectivity of protein kinase inhibitors: A further update. *Biochem. J.* **2007**, *408*, 297–315. [CrossRef]
72. Janaki, A.C.; Sailatha, E.; Gunasekaran, S. Synthesis, characteristics and antimicrobial activity of ZnO nanoparticles. *Spectrochim. Acta Part A Mol. Biomol. Spectrosc.* **2015**, *144*, 17–22. [CrossRef] [PubMed]
73. Modena, M.M.; Rühle, B.; Burg, T.P.; Wuttke, S. Nanoparticle Characterization: What to Measure? *Adv. Mater.* **2019**, *31*, e1901556. [CrossRef]

74. Vimala, K.; Sundarraj, S.; Paulpandi, M.; Vengatesan, S.; Kannan, S. Green synthesized doxorubicin loaded zinc oxide nanoparticles regulates the Bax and Bcl-2 expression in breast and colon carcinoma. *Process. Biochem.* **2014**, *49*, 160–172. [CrossRef]
75. Heim, S.; Mitelman, F. *Cancer Cytogenetics: Chromosomal and Molecular Genetic Aberrations of Tumor Cells*; John Wiley & Sons: Hoboken, NJ, USA, 2015.
76. Alaraby, M.; Annangi, B.; Hernández, A.; Creus, A.; Marcos, R. A comprehensive study of the harmful effects of ZnO nanoparticles using Drosophila melanogaster as an in vivo model. *J. Hazard. Mater.* **2015**, *296*, 166–174. [CrossRef]
77. Chen, P.; Wang, H.; He, M.; Chen, B.; Yang, B.; Hu, B. Size-dependent cytotoxicity study of ZnO nanoparticles in HepG2 cells. *Ecotoxicol. Environ. Saf.* **2019**, *171*, 337–346. [CrossRef]
78. Erdogan, O.; Abbak, M.; Demirbolat, G.M.; Birtekocak, F.; Aksel, M.; Pasa, S.; Cevik, O. Green synthesis of silver nanoparticles via Cynara scolymus leaf extracts: The characterization, anticancer potential with photodynamic therapy in MCF7 cells. *PLoS ONE* **2019**, *14*, e0216496. [CrossRef] [PubMed]
79. Nair, A.; Jayakumari, C.; Jabbar, P.; Jayakumar, R.; Raizada, N.; Gopi, A.; George, G.S.; Seena, T. Prevalence and associations of hypothyroidism in Indian patients with type 2 diabetes mellitus. *J. Thyroid Res.* **2018**, *2018*, 5386129. [CrossRef]
80. Aynalem, S.B.; Zeleke, A.J. Prevalence of diabetes mellitus and its risk factors among individuals aged 15 years and above in Mizan-Aman town, Southwest Ethiopia, 2016: A cross sectional study. *Int. J. Endocrinol.* **2018**, *2018*, 9317987. [CrossRef] [PubMed]
81. Thiruvengadam, M.; Chung, I.-M.; Gomathi, T.; Ansari, M.A.; Khanna, V.G.; Babu, V.; Rajakumar, G. Synthesis, characterization and pharmacological potential of green synthesized copper nanoparticles. *Bioprocess. Biosyst. Eng.* **2019**, *42*, 1769–1777. [CrossRef] [PubMed]
82. Vasudeo, K.; Pramod, K. Biosynthesis of nickel nanoparticles using leaf extract of coriander. *Biotechnol. Ind. J.* **2016**, *12*, 1–6.
83. Weller, J.; Budson, A. Current understanding of Alzheimer's disease diagnosis and treatment. *F1000Research* **2018**, 7. [CrossRef] [PubMed]
84. Khalil, A.T.; Ayaz, M.; Ovais, M.; Wadood, A.; Ali, M.; Shinwari, Z.K.; Maaza, M. In vitro cholinesterase enzymes inhibitory potential and in silico molecular docking studies of biogenic metal oxides nanoparticles. *Inorg. Nano Met. Chem.* **2018**, *48*, 441–448. [CrossRef]
85. Hassan, D.; Khalil, A.T.; Saleem, J.; Diallo, A.; Khamlich, S.; Shinwari, Z.K.; Maaza, M. Biosynthesis of pure hematite phase magnetic iron oxide nanoparticles using floral extracts of *Callistemon viminalis* (bottlebrush): Their physical properties and novel biological applications. *Artif. Cells Nanomed. Biotechnol.* **2018**, *46* (Suppl. 1), 693–707. [CrossRef]
86. Šinko, G.; Vrček, I.V.; Goessler, W.; Leitinger, G.; Dijanošić, A.; Miljanić, S. Alteration of cholinesterase activity as possible mechanism of silver nanoparticle toxicity. *Environ. Sci. Pollut. Res.* **2014**, *21*, 1391–1400. [CrossRef]
87. Sergiev, I.; Todorova, D.; Shopova, E.; Jankauskiene, J.; Jankovska-Bortkevič, E.; Jurkonienė, S. Exogenous auxin type compounds amend PEG-induced physiological responses of pea plants. *Sci. Hortic.* **2019**, *248*, 200–205. [CrossRef]
88. Mohamed, H.I.; Akladious, S.A. Changes in antioxidants potential, secondary metabolites and plant hormones induced by different fungicides treatment in cotton plants. *Pestic. Biochem. Physiol.* **2017**, *142*, 117–122. [CrossRef] [PubMed]
89. Rehman, M.; Ullah, S.; Bao, Y.; Wang, B.; Peng, D.; Liu, L. Light-emitting diodes: Whether an efficient source of light for indoor plants? *Environ. Sci. Pollut. Res.* **2017**, *24*, 24743–24752. [CrossRef] [PubMed]
90. Prieto, M.; Curran, T.P.; Gowen, A.; Vázquez, J.A. An efficient methodology for quantification of synergy and antagonism in single electron transfer antioxidant assays. *Food Res. Int.* **2015**, *67*, 284–298. [CrossRef]
91. Skonieczna, M.; Hudy, D. Biological activity of Silver Nanoparticles and their applications in Anticancer Therapy. *Silver Nanoparticles Fabr. Charact. Appl.* **2018**, 131. [CrossRef]
92. Ul-Haq, I.; Ullah, N.; Bibi, G.; Kanwal, S.; Ahmad, M.S.; Mirza, B. Antioxidant and cytotoxic activities and phytochemical analysis of Euphorbia wallichii root extract and its fractions. *Iran. J. Pharm. Res. IJPR* **2012**, *11*, 241.
93. Khalil, A.T.; Ovais, M.; Ullah, I.; Ali, M.; Shinwari, Z.K.; Hassan, D.; Maaza, M. *Sageretia thea* (Osbeck.) modulated biosynthesis of NiO nanoparticles and their in vitro pharmacognostic, antioxidant and cytotoxic potential. *Artif. Cells Nanomed. Biotechnol.* **2018**, *46*, 838–852. [CrossRef]
94. Nasar, M.Q.; Khalil, A.T.; Ali, M.; Shah, M.; Ayaz, M.; Shinwari, Z.K. Phytochemical analysis, Ephedra Procera CA Mey. Mediated green synthesis of silver nanoparticles, their cytotoxic and antimicrobial potentials. *Medicina* **2019**, *55*, 369. [CrossRef]
95. Das, R.K.; Brar, S.K.; Verma, M. Checking the biocompatibility of plant-derived metallic nanoparticles: Molecular perspectives. *Trends Biotechnol.* **2016**, *34*, 440–449. [CrossRef] [PubMed]
96. Ahmad, F.; Ashraf, N.; Ashraf, T.; Zhou, R.-B.; Yin, D.-C. Biological synthesis of metallic nanoparticles (MNPs) by plants and microbes: Their cellular uptake, biocompatibility, and biomedical applications. *Appl. Microbiol. Biotechnol.* **2019**, *103*, 2913–2935. [CrossRef] [PubMed]